PolyPublie
Polytechnique Montréal

POLYTECHNIQUE MONTRÉAL
UNIVERSITÉ D'INGÉNIERIE

Titre: Title:	Sonochemical Synthesis of Porous Gold Nano- and Micro-Particles in a Rosette Cell
Auteur: Author:	Ndifreke Usen
Date:	2021
Type:	Mémoire ou thèse / Dissertation or Thesis
Référence: Citation:	Usen, N. (2021). Sonochemical Synthesis of Porous Gold Nano- and Micro-Particles in a Rosette Cell [Master's thesis, Polytechnique Montréal]. PolyPublie. https://publications.polymtl.ca/9151/

Document en libre accès dans PolyPublie
Open Access document in PolyPublie

URL de PolyPublie: PolyPublie URL:	https://publications.polymtl.ca/9151/
Directeurs de recherche: Advisors:	Daria Camilla Boffito, & Xavier Banquy
Programme: Program:	Génie chimique

Ce fichier a été téléchargé à partir de PolyPublie, le dépôt institutionnel de Polytechnique Montréal
This file has been downloaded from PolyPublie, the institutional repository of Polytechnique Montréal

https://publications.polymtl.ca

POLYTECHNIQUE MONTRÉAL

affiliée à l'Université de Montréal

Sonochemical Synthesis of Porous Gold Nano- and Micro-particles in a Rosette Cell

NDIFREKE USEN

Département de génie chimique

Mémoire présenté en vue de l'obtention du diplôme de *Maîtrise ès sciences appliquées*

Génie chimique

Mai 2021

© Ndifreke Usen, 2021.

POLYTECHNIQUE MONTRÉAL

affiliée à l'Université de Montréal

Ce mémoire intitulé :

Sonochemical Synthesis of Porous Gold Nano- and Micro-particles in a Rosette Cell

présenté par **Ndifreke USEN**

en vue de l'obtention du diplôme de *Maîtrise ès sciences appliquées*

a été dûment accepté par le jury d'examen constitué de :

Mario JOLICOEUR, président
Daria Camilla BOFFITO, membre et directrice de recherche
Xavier BANQUY, membre et codirecteur de recherche
Nick VIRGILIO, membre
Ines Esma ACHOURI, membre externe

DEDICATION

To Philippe who influenced and supported me from miles away through the rough and smooth times.

To California and Walnut. Finally, to my family for their support and love.

ACKNOWLEDGEMENTS

I would like to express my fortune at completing my graduate studies at Polytechnique de Montreal. However, without the consent of my supervisor, Dr. Daria-Camilla Boffito who accepted me to work in her lab and supported me through my research, none of the experience I have garnered would have been possible. I am very grateful for her supervisory approach, her knowledge and expertise in the subject area which provided me the background I required as well as enabled me to work independently on my research. Also, for providing an opportunity to work as a team on other outstanding projects which greatly enriched my research activities and enhanced my collaborative endeavors.

I would like to thank my co-supervisor Dr. Xavier Banquy and the PrEEmium group (Process Engineering of Emerging Nanomedicines) for the opportunity to be part of a growing network of scientists and engineers pioneering the research and development of nanomedicines. To my co-supervisor, I would like to express my appreciation for being a source of knowledge that guided my research activities.

Special thanks to Claire Cerclé for training me on several of the instruments used to characterize my results as well as for her kindness. I would also like to express my gratitude to members of the Centre for Characterization and Microscopy of Materials (CM2) for help in imaging of my samples and providing feedback on the characterization.

To our lab members, for being a source of inspiration and a sounding board for ideas. Special acknowledgement to Hela Laajimi and Mahmoud Zorainy amongst others for your kindness, and friendship.

Last but not the least, I am grateful to my life partner for his encouragement and to my family who in their own way gave me the strength required to complete my research.

RÉSUMÉ

La demande pour des nanoparticules d'or s'explique par le fait qu'elles sont biocompatibles et possèdent des propriétés physiques et chimiques adaptées à une application théranostique (thermodiagnostic). . La possibilité d'ajuster leur tailler à l'échelle nanométrique leur permet de pénétrer dans les cellules et les tissus, tandis que le contrôle de leur forme permet d'imiter les virus ou d'accéder aux différents canaux du corps. À titre d'exemple, les nanoparticules cavitaires peuvent permettre le chargement d'agents thérapeutiques appliqués dans l'administration de médicament ou pour l'imagerie contrastée améliorant ainsi la capacité de diagnostic. La modification de la surface des nanoparticules à l'aide de polymère furtifs permet aux nanomatériaux d'éviter la détection ainsi que la possibilité d'attacher différentes molécules/ligands. Toutes ces propriétés rendent les nanoparticules d'or essentielles au traitement de plusieurs maladies, d'où l'importance de synthétiser des d'or nanomatériaux de différentes tailles et formes.

Nos travaux ont eu pour objectif de produire des nanoceintures d'or en appliquant un ultrason à basse fréquence (20 kHz) comme méthode de synthèse. Nous avons choisi une biomolécule (le glucose) comme agent réducteur et de couverture pour éviter la contamination du produit final et permettre ainsi son application en diagnostic et en thérapie. La méthode de synthèse implique l'utilisation d'ultrasons pour générer des radicaux capables de réduire les ions d'or (Au3+) en nano-or (Au). Une boucle du réacteur à cellules en rosette favorise la cavitation hydrodynamique tandis que la cavitation acoustique est générée par le mouvement de la corne à ultrasons. L'efficacité sonochimique s'est avérée plus élevée avec des ultrasons continus qu'avec des ultrasons intermittents. La réduction des nanoparticules d'or nécessite des radicaux hydroxyle générés par la sonolyse de l'eau et la pyrolyse du glucose. De plus, un environnement à pH élevé conduit à de l'agglomération tandis qu'un pH faible donne des formes anisotropes. Les nanoparticules d'or ainsi synthétisées sont caractérisées par MEB, EDS, DRX et IR-TF. À notre connaissance, c'est la première fois que la synthèse de nanoparticules d'or dans une cellule en rosette utilisant l'eau comme solvant et une biomolécule comme agent réducteur à 20 kHz a été signalée.

ABSTRACT

The demand for gold nanoparticles stems from the fact that they are bio-compatible and possess physical and chemical properties suitable for theragnostic application. The ability to tune their size at the nanoscale enables them to penetrate cells and tissues while control of their shape enables virus mimicry or access to different channels in the body. For example, hollow nanoparticles may enable the loading of therapeutic agents towards drug delivery applications or for image contrast thereby improving diagnostic abilities. Surface modification of nanoparticles with stealth polymers allows for nanomaterials to avoid detection as well as the ability to attach different molecules/ligands. Together these properties allow for gold nanoparticles to be essential in the treatment of several diseases and hence the importance of synthesizing gold nanomaterials of different sizes and shapes.

In our work, we synthesized Au NPs and porous Au MPs by applying low frequency ultrasound (20 kHz) as a synthesis method. We chose a biomolecule (glucose) as a reducing and capping agent to avoid contamination of the final product thus enabling its application in diagnosis and therapy. The synthesis method involves the use of ultrasound to generate radicals capable of reducing gold ions (Au^{3+}) to nanogold (Au). Hydrodynamic cavitation is promoted by loops of the rosette cell reactor while acoustic cavitation is generated from the movement of the ultrasound horn. The sonochemical efficiency was found to be higher with continuous than intermittent ultrasound. The reduction of gold nanoparticles requires hydroxyl radicals generated from water sonolysis and glucose pyrolysis. Furthermore, a high pH environment led to agglomeration while, low pH results in anisotropic shapes. The as synthesized gold nanoparticles are characterized by SEM, EDS, XRD and FT-IR. To the best of our knowledge this is the first time that the synthesis of gold nanoparticles in a rosette cell employing water as a solvent and a biomolecule as a reducing agent at 20 kHz has been reported.

TABLE OF CONTENTS

LIST OF TABLES

LIST OF FIGURES

LIST OF SYMBOLS AND ABBREVIATIONS

AA	Ascorbic acid
$AgNO_3$	Silver nitrate
Au	Gold
Au^{3+}	Gold ion
Au NB	Gold nanobelt
Au NCg	Gold nanocage
Au NC	Gold nanoclusters
Au NH	Gold nanohexapod
Au NRs	Gold nano-raspberries
Au NSh	Gold nanoshells
Au NS	Gold nanosphere
Au NR	Gold nanorods
Au NP	Gold nanoparticle
$C_6H_{12}O_6$	α-D-glucose
Cl^-	Chlorine ion
CTAB	cetyl trimethylammonium bromide
CTAC	cetyltrimethylammonium chloride
DA	Dopeamine
EDX	Energy dispersive X-ray
FA	Folic acid
FE SEM	Field emission scanning microscopy
FT-IR	Fourier transform – Infra red
$HAuCl_4$	Gold tetrachloride

HCl	Hydrochloric acid
$NaBH_4$	Sodium borohydride
NaOH	Sodium hydroxide
NIR	Near infrared region
PEG	Polyethylene glycol
PG	Pineapple gum
pH	Hydrogen potential
PTT	Photothermal therapy
PVP	polyvinylpyrrolidone
RM	Reverse micelle
RPM	Rotation per minute
SPR	Surface plasmon resonance
TEM	Transmission electron microscopy
UV-Vis	Ultraviolet-Visible spectrum
US	Ultrasound
XRD	X-ray powder diffraction

LIST OF APPENDICES

CHAPTER 1 INTRODUCTION

1.1 Context

Gold which is one of the first metals to have been discovered is recently seeing a dramatic resurgence in biomedical applications [1]. Gold nanoparticles are nano sized particles formed from elemental gold (Au). Their extensive use in various applications stems from properties conferred by their size, shape and environment. Gold nanoparticles exhibit beneficial properties such as a high surface to volume ratio at the nanoscale compared to their bulk counterparts. They are biocompatible, stable, non-corrosive, and can easily be functionalized with different molecules while possessing low toxicity when absorbed into cells. Therefore, their synthesis and characterization are highly relevant for applications in disease diagnosis, therapy and drug delivery.

One key application of gold nanoparticles is in cancer theragnostic, an emerging concept intended to combine both therapy and diagnostic without damaging healthy cells [2]. Cancer represents a leading health problem because of the lack of an effective universal treatment and in 2020 an estimated 225 800 new cancer cases and 83 300 cancer deaths are expected in Canada alone [3]. Though many cancers can be removed surgically if caught early and treated to some degree through radiation, chemotherapy, or immunotherapy, at present the treatment of cancer remains a patchwork of different drugs, surgeries, and therapies, none of which can fully remove advanced forms of the disease [4]. As a result, new cancer treatments remain at the forefront of medical research in many regards, and gold nanoparticles offers one of the most promising lines of research in this regard due to their non-toxicity, ability to act as a targeted drug carrier [5] and possession of SPR suitable for tumor ablation[6]

Figure 1-1 Basic properties of Au NPs and their application in cancer therapy

To capitalize on the intrinsic properties of Au NPs, researchers have focused on the synthesis of Au NP based on two different approaches. The first approach involves physical or mechanical methods of reducing bulk Au to nano size (1-100 nm). This approach is limited by the lack of shape and size control as well as extensive synthesis times. On the other hand, bottom-up approaches mostly used in chemical and biological methods try to build the Au NP from smaller molecules utilizing reducers and stabilizers to achieve precise control of shape and size. However, the use of toxic or hazardous materials during the synthesis process may hinder the biocompatibility and stability of the resulting Au NPs. As a result, several methods utilizing either biological or eco-friendly agents to control the nucleation process have been developed.

On the other hand, most synthesis methods result in the formation of spherical gold nanoparticles while little attention has been paid to microparticles which are less toxic compared to their nanoscale counterparts. Au MPs possess plasmonic properties and can interact with light based on a combination of bulk metallic characteristics (e.g., thermal conductivity and ductility) and nanometric size-effect properties (e.g., plasmonic behavior, and high surface area) making them suitable for targeted cancer drug delivery [7]. However, their synthesis has received less attention, owing to experimental difficulties such as tedious multistep procedure and time-consuming gelation time [8].

Sonochemistry which is the use of sound waves to enhance chemical reactions has been explored for the synthesis of gold nanoparticles. Ultrasound baths are commonly used in the reduction of gold precursors at frequencies between 37 – 950 kHz. To control the shape and size of the gold nanoparticles, researchers tune ultrasound parameters of time and power while varying synthesis parameters such as surfactants, alcohols or pH in the presence of inert gases such as Ar. The work of this thesis is derived from this simple, eco-friendly and biocompatible process to synthesize gold nanoparticles at 20 kHz.

1.2 Objective

The general objective of this research proposal is to assess whether a 20 kHz ultrasound can be used as a synthesis method for the preparation of biocompatible gold nanoparticles. In accordance with the research question, we aim to develop a sonochemical method to synthesize glucose stabilized gold nanoparticles by direct probe sonication in a rosette cell reactor. If successful, to relate the process parameters with the optical and morphological properties of the obtained nanoparticles.

1.3 Dissertation Plan

This master's dissertation is divided into five chapters. Chapter 2 presents the literature review focusing on gold nanoparticle applications and their synthesis methods. Chapter 3 describes experimental and analytical procedures implemented in this study. Chapter 4 presents a summary of the main results of this work in the form of a scientific article most recently submitted for publication in a scientific journal. General discussion is presented in chapter 5 and finally conclusion and future recommendation are presented in Chapter 6.

CHAPTER 2 LITERATURE REVIEW ON THE APPLICATION AND SYNTHESIS OF GOLD NANOPARTICLES

2.1 Application of Gold Nanoparticles

Gold (Au) is one of the first elements to have been discovered. Its symbol in the periodic table is Au and it has one of the higher atomic numbers of transition elements: 79. Bulk Au's is stable, malleable and the least chemically reactive of the transition elements [7]. Bulk gold is chemically inert due to strong suppression by neighboring gold atoms [8] and is characterized by x-ray diffraction as having a face centered cubic crystal [9]. The earliest use of gold for medical purposes is traced back to the Chinese and Egyptian civilizations around 2500 BC whereby gold was used in the treatment of diseases such as syphilis and measles [10] Since then, gold nanoparticles have been applied in treatment of rheumatoid arthritis and currently as nanocarriers for theranostics [11]. Au NPs are nano sized particles formed from the reduction of bulk Au. Compared to bulk Au which has a yellow color, Au NPs exhibit a variety of colors (ranging from red to violet) and shapes (nanospheres, nanowires, nanobelts, nano triangles, nano-stars) depending on their surface plasmon resonance which occurs at specific wavelengths. As a consequence of their small size and variety of shapes they have particular relevance in biomedical applications because of a large surface-to-mass ratio, an ability to act as carriers of other particles, and a low toxicity when absorbed into cells [12]. For instance, their light scattering property is used in cell imaging [13] while their ability to absorb light and convert it to heat is applied in photothermal therapy to destroy cancer cells [14]. For drug delivery, the surface of gold nanoparticles can be easily functionalized with different molecules to target specific cells thus enhancing the therapeutic dose. Therefore, AuNPs are an important biomedical tool, and their synthesis is highly relevant from a functional perspective.

2.2 Synthesis of Gold Nanoparticles

Several developed methods are available to synthesize Au NPs. Typically, methods follow either a top-down approach where bulk gold is broken down to small sizes (Figure 2-1A) or a bottom-up approach where gold atoms are built up layer by layer to produce nanoparticles of desired sizes and shape (Figure 2-1B). While both approaches can produce nanoparticles of desired shapes and sizes, they have limitations. For example, top-down approaches lead to extensive waste of materials while bottom-up approaches have poor size distribution or make use of hazardous reagents in the synthesis process [15]. The two approaches can be further divided into physical, chemical and biological methods.

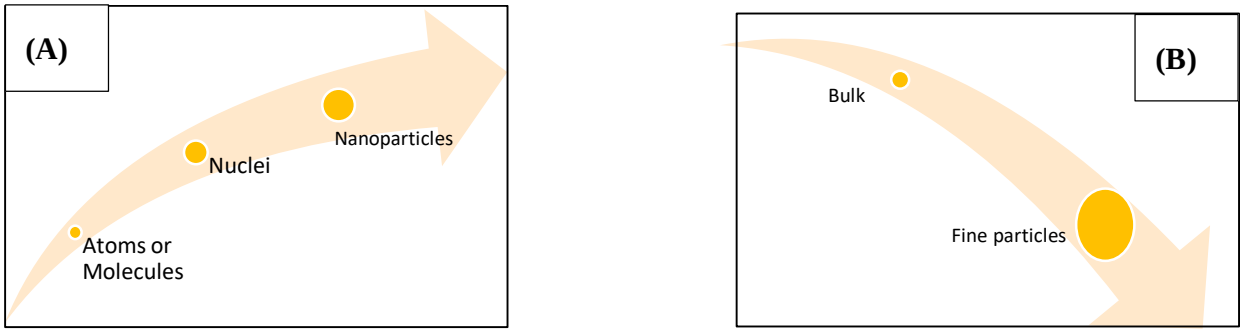

Figure 2-1 (A) Bottom-up and (B) Top-down approaches for the synthesis of AuNPs.

2.2.1 Physical Methods

This method is based on the reduction of bulk gold when it is irradiated by ionizing (x-rays and gamma rays) or non-ionizing (microwave and ultraviolet) irradiation which leads to particle nucleation [16]. The various physical nanoparticle synthesis techniques are solid-state technique, vapor phase synthesis, and laser ablation technique. For example, laser irradiation provides an approach to assist the reshaping, fragmentation and assembly of AuNPs. Although this method typically produces spherical nanoparticles, Pioto et al have described a method for the production of anisotropic Au NPs by repetition of laser ablation of a gold target in aqueous sodium chloride as solvent [17]. During the first round of laser ablation, spherical Au NPs were produced. However, recirculation of the products and further laser ablation led to the production of anisotropic Au NPs.

2.2.2 Chemical Methods

Synthesis of gold nanoparticles via the chemical reduction method involves the use of a reducing agent (citric acid or sodium borohydride) that reduce the oxidize of Au ions from an oxidation state of +3 to 0 which is the oxidation state of Au atoms. Secondly, stabilizers such as sodium citrate, sulfur ligands (mostly thiolates), polymers or surfactants (CTAB) are added to control the size or shape of the reduced gold atoms and to prevent aggregation [16]. It is possible that stabilizers can play a dual role of reduction and stabilization as is in the case for trisodium citrate [18]. The production of monodisperse gold nanoparticles is dependent on several factors such as reaction temperature, stirring rate, the ratio of gold to reducing agent as well as careful cleaning of glassware. For example, the most commonly used chemical method for gold nanoparticle production is the Tukervitch synthesis [19]. To synthesize gold nanoparticles with average sizes of 10 nm, the gold precursor is heated to boiling temperature and then trisodium citrate is added to reduce the gold atoms while citrate acts as a stabilizer preventing aggregation [20]. Recently, Gutierrez et al. modified a reversed micelle (RM) method to obtain several different morphologies [21]. This synthesis method resulted in the formation of Au NPs of different shapes as evaluated by UV-Vis and TEM. The Au NP sizes were around 26 nm, depending on the shape, with rings of 16–18 nm. Although there was a wide particle shape distribution, these results are applicable in photothermal cancer treatment due to their observed anisotropy. A novel way of AuNP modification involved the in-situ formation of folic acid-derived structures on AuNP surface via a one-step hydrothermal treatment [22]. FA capped AuNPs (FA-AuNPs) are used for targeting, imaging, and site-specific therapy because cancer cells over-express folate receptors, making Au NPs modification with FA a suitable candidate for cancer therapy. The Au-NPs were synthesized by reducing Au ions with sodium citrate and then functionalized with FA. The results showed that the hydrodynamic diameter of FA-Au NPs was 38 nm compared to 36 nm which was obtained from hydrothermally treated AuNPs. FA-AuNPs retained properties of precursor molecules and the biological ligand thus ensuring specific binding to anti-FA antibody. Au NPs were synthesized using aspartic acid as a reducing and capping agent after nine hours [23]. In general, chemical reduction method involves the use of multiple steps, hazardous reagents and are time consuming

for the synthesis of Au NPs. Although there are abundant uses of isotropic Au NP, the synthesis of anisotropic Au NP is gaining momentum. This is because they can absorb in the near-infra-red window which optimal optical window for nanomedicine applications. The synthesis of anisotropic Au NPs, involves two strategies, a seedless and seeded based method. Currently, both of these methods use cetyltrimethylammonium bromide (CTAB), which is cytotoxic [24] and can cause developmental abnormalities in living organisms thus presenting an ecological risk [25]. Therefore, there is a need to develop eco-friendly and biocompatible synthesis routes for anisotropic Au NPs such as Au NRs, and Au NBs.

2.2.2.1 Seed based methods

In seed-based methods, Au NPs are used as templates and centers for further nucleation, producing a wide diversity of morphologies [25]. Generally, for anisotropic NP synthesis, an Au seed solution is prepared with a reduction of $HAuCl_4$ in CTAB, using $NaBH_4$ as reducing agent. The reaction medium is stirred vigorously to grow the Au seeds phase. Finally, the seed solution is mixed with $HAuCl_4$ in CTAB and $AgNO_3$, to produce anisotropic nanoparticles [26]. Variation in nanoparticle size is achieved by changing the concentration of reactants, or the stabilizing agents. Au NPs were synthesized via photoreduction in a seeded method using hydroquinone as the reducing agent [27]. The seed solution was prepared after two hours of constant stirring before use as a template. The seed and growth solutions were irradiated with visible light at 0.75 W cm^{-2} to form Au NPs. The authors note that the pH of the reducing agent solution was important for the synthesis of Au NPs.

2.2.2.2 Seedless methodologies

Seedless methods produce smaller Au NPs than those obtained using a seed-based methodology. For instance, biocompatible Au NW suitable for PTT were synthesized in a one -step protocol [28]. Au ions were first reduced by $NaBH_4$, followed by fusion of Au atoms assisted by DA. DA acted as the structure directing agent which can also undergo polymerization to form a layer of coating on the Au NW surface. Au NPs were also produced in a one-step method through polyol reduction at alkaline conditions [29]. In this case, the addition of PVP or CTAC stabilization agent was necessary to prevent aggregation of Au NPs. Although this method is simple and fast, it however involves the use of a strong and hazardous reducing agent $NaBH_4$ or the use of a cytotoxic material CTAC which requires further purification before biomedical application.

2.2.3 Biological Methods

This method is a clean, nontoxic, and eco-friendly approach for the synthesis of Au NPs. A wide range of biological agents such as biopolymers, enzymes, bacteria, fungi and plant are employed as reducing agents [30]. For instance, bacteria can adsorb and accumulate metals, however only a few can selectively reduce metal [31]. Plant extracts can reduce and adsorb on the surface of Au NPs. The drawback with this method is that the reducing component is not always known, and some methods involve long preparation times [32].

A broth of the leaf and stem of C. quadrangularis was employed as both the reductant and stabilizer in the synthesis of biocompatible Au NPs [33]. The authors note that the reducing properties of the polysaccharide ends were involved in the reduction of $[AuCl_4]^-$ to Au. PG chains were involved in the stabilization of Au NPs, over a period of two months. The Au NPs-PG were non-toxic to human blood cells in vitro making them hemo-compatible. However, synthesis via the plant route is limited by long plant preparation required to obtain the bioactive constituents necessary to reduce and stabilize the Au NPs.

2.3 Gold Nanoparticle synthesis by ultrasound

Ultrasound processing is an environment-friendly, safe and inexpensive technology, that has a wide range application in biology, chemistry, medicine and material science. Inorganic nanomaterials can be synthesizing or modified using ultrasonic irradiation. The acoustic cavitation produced by ultrasound in water results in the formation and violent collapse of microbubbles, which plays an essential role in the formation of the nanostructure. Therefore, the physical and chemical phenomena generated by ultrasonic irradiation can produce conditions necessary for reagent-free reduction of gold ions and the formation of particles in different shapes and sizes [34].

The sonochemical route which generates cavitation arises from high temperature and local pressure (physical effect), produces hydrogen and hydroxyl radicals from water sonolysis (chemical effect) or pyrolysis of molecules, as shown Eq. (1). Consequently, the reduction of Au(III) ions in aqueous solution occurs by ·H radicals, from water molecules or methyl radicals , followed by nucleation of Au(0) into AuNPs, as shown the Eq. (2).

H_2O + ultrasound → e_{aq}^-, H_3O^+, $H^\bullet$, H_2, $OH^\bullet$, H_2O_2 Eq. (1)

Au(III) (+by ·H, CH_3) → Au(0) → AuNPs Eq. (2)

The bubbles formation, their growth, and final implosion induces hot spot regions with high internal local temperatures and high pressure. With these conditions, the reactants have intensive interactions in extremely short time-lapse, resulting in fast heating and cooling rates, thereby improving sonocrystallization. Therefore, the interaction between irradiation energy and the irradiated solution is key to controlling the properties of the prepared Au NPs [35].

A challenge in the sonochemical routes for Au NPs preparation is to control the morphology, particle size distribution, and crystalline structure. Several strategies have been proposed to control these properties, such as changing metal concentration, using different alcohols, surfactants, and gas. Besides that, it is possible to vary the ultrasonic power [34], [35].

In addition, during the sonochemistry process, a reducing agent is usually added to facilitate the formation of the nanoparticle. Some of the reducing agents mostly used, are sodium borohydride ($NaBH_4$) or hydrazine that are hazardous [36]–[39]. Recently, 1-butanol was applied as a reducing agent, the authors observed that the reduction rate of of Au precursor and radical formation increased with 1-butanol concentration. However, at 5 mM concentration, the Au reduction decreased and consequently the formation of radicals decreased [40]. It is possible to prepare Au NPs with different sizes by modifying the ratio of Au precursor with the reducing agent to control nucleation velocity and steric surface. Optimized concentration of the reducing agent accelerates the reduction rate of Au(I) resulting in a change in shape of Au nanoparticles.

Chemical effects of ultrasound irradiation were suggested in the disproportionation process whereby electrons of $AuCl_4^-$ are rapidly desorbed from a tetrachloroaurate complex ($HAuCl_4$) and recycled for the two-electron reduction by the reducing agent. Subsequent aurophilic interaction between $AuCl_2^-$ complexes, electrons exchange and catalytic growth of gold seeds, result in the deposition of new gold atoms on the surface promoting the growth of Au NPs. These mechanisms are enhanced by the effects of ultrasound, such as cavitation and transmitted energy into the

solution. Okitsu et al., studied the variation of $HAuCl_4$ concentration, and reported that the Au changed its morphology to nanorods with increasing $HAuCl_4$ concentration in the range of the conditions investigated in that study, highlighting that the concentration balance between $HAuCl_4$ and the reducing agent was important to proceed the reduction of Au (I) effectively [39].

Another very important constituent for the development of gold nanoparticles is the use of surfactants such as silanol or alcohol as a capping agent. Park et al., studied several concentrations of sodium dodecylsulfate (SDS), as a capping agent. They conclude that the shape and size of Au NPs depend on the ratio of HAuCl4/SDS, decreasing as the proportion decreases. Thus, the size of Au NPs decreased with an increase of SDS and spherical type of Au NPs was observed at a high concentration of SDS. Wei et al., described the use of 3-Glycidoxypropyltrimethoxysilane (GPTMS) in the sonochemical formation of gold nanoparticles. GPTMS tend to fuse with each other as the condensation of silanols occurs, forming worm or nugget-like gold nanostructures. The use of long-chain surfactants, as polyethyleneglycol (PEG), inhibited the fusion, leading to mono-dispersed Au NPs. They affirm that the higher GPTMS concentration decreases the Au NPs size which suggests that GPTMS adsorb onto the surface of Au NPs [41].

Some operational conditions can also alter the formation of nanoparticles, without changing the synthetic parameters. The different irradiation powers influence the size and shape control parameters. For example, Park et al., studied the formation of Au NPs using ultrasonic radiation range between 30 W to 90W and conclude that the irradiation by high power ultrasound leads to the enhancement of the formation of reactive radical species, therefore the high-power ultrasound rapidly promotes the reduction of Au ion when it is compared to the low power ultrasound. Thus, the high power provides Au NPs smaller than the Au NPs obtained at low power and, besides that, the shape of nanoparticles changed from multiple to spherical with increasing ultrasonic irradiation power [42].

Another parameter that can interfere with the synthesis result is the gas used in the reaction medium. The effect of dissolved gas on the size and shape of Au NPs prepared using the sonochemical reduction method was studied by Sakai and collaborators. They used Argon (Ar), Nitrogen (N_2), Oxygen (O_2), and Hydrogen (H_2) gases as purged gas. The size and shape of NP are determined by a competition between nucleation (metal ion reduction on nuclei) processes so that the increase in the amount of reducing species ($H\cdot$) should lead to the formation of smaller particles

due to the increase of reduction sites. Therefore, the formation of smaller spherical Au NPs in H_2-purged aqueous $AuCl_4^-$ solution would be attributed to the increase in the amount of reducing species (H·) due to the reaction of H_2 with OH· generated from sonolysis of water as follows. It is known that the reaction indicates the generation of H· by rebinding of OH· with H_2·, which implies that the generation of H· during the sonication is promoted in the presence of H_2. The introduction of H_2 gas into an aqueous $AuCl_4^-$ solution would promote the reaction of OH. with H_1 and resulting generation of H· (that acts as a reducing species of $AuCl_4$). As result, smaller spherical Au NPs would be formed in the H_2-purged aqueous $AuCl_4$ solution. In the presence of O_2 in an aqueous solution, H· would be scavenged by O_2, so the amount of H· should be smaller than that in the absence of O_2 in the solutions, resulting in a larger particle. Ar and N_2 gas do not interact with hydrogen radicals, then the size and shape of Au NPs formed would not be affected by the introduction of gas into the aqueous solution, forming similar size and shape. Thus, the use of H_2 gas should provide benefits in the production of the pure metal nanoparticles, because H_2 produces only water after reaction while the conventional method typically normally produces toxic products from the reaction of metal ions with reducing agents ($NaBH_4$, hydrazine, and citric acid)[38].

The sonoelectrochemistry method to prepare gold nanoparticles is currently explored by several manuscripts. This technique is promising because it allows the synthesis of Au NPs by adjusting size and shape without altering the experimental condition, which is extremely positive to scale-up to industrial production. The electrodeposition combined with high intensity of ultrasound pulses was proposed to prepare a large number of NPs with a narrow size distribution (10- 50 nm). This method is accomplished by applying an electric current pulse to nucleate and perform the electrodeposition, followed by a burst of ultrasonic waves to remove the products from the sonic probe cathode. The shape and size can be controlled by adjusting various parameters such as current density, time of deposition and sonication, temperature, pH, and pulse. The size of Au NPs increases with an increase of the current pulse time, while high reaction times results in uniform size distribution as well as decrease in particle size. Besides that, well-dispersed Au NPs can be synthesized at basic conditions (pH 10 the surface potential is -54 mV), indicating that the OH- groups adsorbed on Au NPs surface cause the electrostatic repulsion, thus preventing aggregation[43].

Fuentes- García et al., studied the ultrasound (20KHz) irradiation power to control the size and shape of nanoparticles. The Au NPs colloidal suspension were obtained using chloroauric acid ($HAuCl_4$) and trisodium citrate (Na_3Ct) under continuous irradiation. The synthesis was described adding 50 mL of $HAuCl_4$ (0.025mM) into a 100 mL beaker, which was added 1 mL of 1.5 % (w/v) aqueous solution of Na_3Ct under 60, 150 and 210 W ultrasonic irradiation power for one hour, at room temperature. The $Na_3Ct/HAuCl_4$ ratio used in the three samples was 3:1 (w/v). A schematic representation of the experimental ultrasonic processing for AuNPs and the sonochemical effects in an aqueous solution is shown in Figure 2-2.

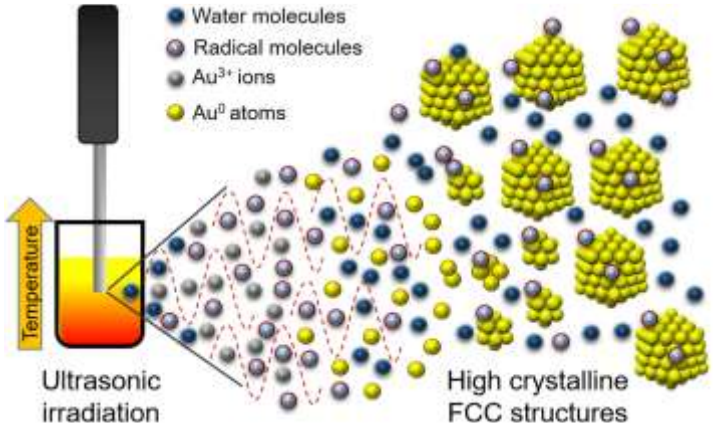

Figure 2-2 Processing of GNPs shows nucleation and growth promoted by sonochemical effect in ultrasonic irradiation in aqueous solution.

This suggested experimental procedure shows the different phenomena involved in the ultrasound-assisted method, associating the physical effects such as temperature and pH rise over the reaction with cavitation phenomena and radical exchange. The results show the strong influence of increasing ultrasound irradiation to the particle size, polyhedral structure, and optical properties of the obtained AuNPs. Particles sizes from 16 nm reached on power setting of 60 and 150W can be reduced to 12 nm using the 210 W. The mechanism can be described in a simple molecular-based scheme, whereby electrons of $AuCl_2^-$ are rapidly exchanged through the gold surface, and after that $AulCl_4^-$ and Cl^- are desorbed, and complex tetrachloroaurate is recycled for the two-electron reduction by citrate[34].

Huynh et al., reported a green and facile method for the preparation of multi-branched gold nanoparticles using hydroquinone as reducing agent, chitosan as a stabilizer, and ultrasound

irradiation to improve the shape and stability. The influence of pH, concentration of chitosan and hydroquinone were investigated. The results showed an average core diameter of 64.85 nm and 76.11 nm of the multi-branched particles[44]

To conclude, the choice of the technique used to synthesize AuNPs depends on the study aim. If the application of Au NPs is biological, the use of sonochemistry can be interesting because it allows a greater variation of parameters to obtain the appropriate material, in addition to the ease of synthesis and low equipment cost. Also, it is possible to modify the operational parameters according to the final goal, such as particle size and shape. For this type of synthesis, it is interesting to use a reducing agent that will accelerate the formation of the nanoparticle without the need for very high ultrasound frequency.

CHAPTER 3 EXPERIMENTAL METHODOLOGY

Briefly, the experimental method involved the use of Gold tetrachloride trihydrate ($HAuCl_4$) as the gold precursor, alpha-d-glucose (α -D - $C_6H_{12}O_6$) as the reducing agent and sodium hydroxide for pH variation. To generate acoustic cavitation, a 20 kHz ultrasound operating at a nominal power of 130 W was used. A rosette cell with loops that create orifices was used as the sonochemical cell to generate hydrodynamic cavitation. Gold microparticles were prepared following a seed-mediated ultrasound assisted method, while gold nanoparticles were prepared via a two-step and a one-step sonochemical method.

3.1 Materials

Gold tetrachloride trihydrate ($HAuCl_4.3H_2O$, 99%), α-D-glucose ($C_6H_{12}O_6$, 99%), and sodium hydroxide (NaOH, 99%) were purchased from Sigma Aldrich (St. Louis, MI, USA) and used as received. Deionized water (DIW) (18MΩ, 4.3 μS/cm, Millipore) was the solvent. Rosette cell reactor and a 20 kHz Vibracell ultrasound processor operating at 130 W from Sonics® & Materials, Inc., (Newtown, CT, USA). The transducer (model CV18) was fitted with a 3 mm diameter probe tip, all obtained from Sonics® & Materials, Inc., (Newtown, CT, USA).

3.2 Synthesis

3.2.1 Seed-mediated sonochemical synthesis of Au MPs

In this experiment, α-D-glucose and NaOH were used to synthesize Au MPs (Figure 4-2). The effect of glucose concentration, pH, order of reagents addition and ultrasound irradiation time on the formation of Au MPs was thoroughly investigated through a series of experiments (Tables 4-1 and 4-2). α-D-glucose was chosen as the reducing agent as further purification of the synthesized Au MP is not required before biomedical application. Furthermore, compared to its stereo isomer, the oxidation product of α-D-glucose which is starch is easily metabolized compared to cellulose which is obtained from β-D-glucose. In the seed solution, before addition of α-D-glucose the Au is

in the form of Au^{3+}. Addition of NaOH changes Au^{3+} to [Au $(OH)_3$]. In the growth solution Au^{3+} is surrounded by the hydroxyl groups from α-D-glucose which serves as a weak reducing agent and prevents aggregation. The application of ultrasound increases the reduction and nucleation of the Au precursor by producing reducing and oxidizing radicals from water and α-D-glucose which binds to the nucleated sites by their carbonyl and hydroxyl ends increasing particle size.

In detail, the seed solution was prepared by mixing 10 mL aqueous solutions of 12.6 mM $HAuCl_4$ with NaOH at concentrations of 38 mM (pH 5), 63 mM (pH 7) and 115 mM (pH 12). Next, growth solutions containing 5 mL aqueous solutions of 12.6 mM $HAuCl_4$ with $C_6H_{12}O_6$ concentrations of 9.9 mM, 19.9 mM and 39.9 mM at pH 2 were prepared and the solutions were yellow in color. The seed solution changes color from yellow to transparent within 30 s with the rate of color change depending on the added amount of NaOH to aqueous 10 mL of 12.6 mM $HAuCl_4$ solutions. Mixing $HAuCl_4$ with NaOH resulted in the formation of Au hydroxide [Au $(OH)_3$], sodium chloride (NaCl) and water. Then the seed solution ($HAuCl_4$ and NaOH) and growth solution ($HAuCl_4$ and $C_6H_{12}O_6$) are mixed together to obtain final pH values of 5, 7 and 12. Following the combination of the seed and growth solutions, probe sonication is applied at a power output of 20 ± 1 W and US power density of 1.3 W mL^{-1} for 30 min. (Figure 4-2). All products were stored in 15 mL centrifuge tubes at 4°C before characterization.

Next, an experimental design was conducted for the production of porous Au MPs which were precipitated at pH 12 (Table 4-2). The effect of mixing sequence (NaOH then $C_6H_{12}O_6$ and vice-versa), sonication time (30 min and 40 min with a mid-point of 35 min) and sonication mode (intermittent vs. continuous) on the nanoparticle size and morphology were explored at a constant power of 20 ± 1W corresponding to an US energy density of 1.3 W mL^{-1}. Mixing the growth and seed solutions yielded a violet solution which, after sonication, became a clear suspension with brown particles sedimenting at the bottom of the rosette cell. For each treatment, the probe position was maintained at approximately 1 cm from reactor. Furthermore, a total energy consumption of ~49,000 J was recorded for all the experimental runs. On the other hand, the difference in recorded total energy from the processor during intermittent or continuous sonication was negligible.

3.2.2 Two step sonochemical synthesis of Porous Au NPs

For the two-step method, the reagents were the same as the seed-mediated method. However, during the first step, probe sonication was continuously applied to aqueous solution-A containing 2 mM $HAuCl_4$ and 100 mM $C_6H_{12}O_6$ inside a rosette cell reactor kept in a thermostatic water bath at 25 ± 1°C. A digital thermometer in the reaction vessel during the sonication process recorded a temperature rise of 5 ± 1°C. Solution-B was prepared by maintaining the same molar ratio of the reagents and ultrasound parameters as in solution-A; however, the DIW volume was increased to 20 mL. The calculated US energy density was 1.0 W mL^{-1} for solution-A and 0.5 W mL^{-1} for solution-B, respectively. This process concluded the first step of the experiment. After 24 h storage at 4 °C, 5 mL of solution-A is mixed with 5 mL of solution-B, followed by the direct probe sonication with an US energy density of 1.1 W mL^{-1} at pH 2. The solution remained yellow and no color change or an appearance of UV-Vis peak were observed after 30 min in that case. Then, a 10 mM solution of NaOH was added dropwise into the mixture under sonication until a violet color was observed, at a corresponding pH of 9. A maximum peak at 563 nm measured by UV-Vis confirmed the formation of Au NPs. Adding excess NaOH changed the color of the suspension from violet to blue at pH 12, and the intensity of the corresponding UV-Vis peak decreased. The solvent volume, reaction time and power delivered from the probe resulted in the formation of Au NPs at pH 9 and potato-shaped gold particles at pH 12 (Table 4-3)

3.2.3 One step sonochemical synthesis of Au NPs

This experiment designed with optimized concentrations of precursor and reducing agents was conducted under continuous ultrasonic irradiation and compared to a conventional chemical synthesis route. In the first scenario, 200 mM $C_6H_{12}O_6$ is pre-mixed with 2 mM $HAuCl_4$ in a synthesis vehicle (rosette cell for ultrasound experiments and a beaker for chemical reduction method). Subsequently, 7.5 mM NaOH is added to the solution undergoing continuous ultrasound irradiation or stirred at 550 RPM for the conventional route. In the second scenario, all reactants are pre-mixed together before applying ultrasound or stirring. After synthesis, the products were analyzed by UV-Vis then stored at 4°C for further characterization.

3.3 Analytical

All colloidal Au NPs were stored at 4°C following synthesis completion before analysis by SEM, XRD and FT-IR, while UV-Vis characterization was performed immediately after synthesis.

3.3.1 UV-Vis

UV-Vis allows for fast and real time monitoring of Au NP size, concentration and aggregation. It does not require extended sample preparation which could change the optical properties of as synthesized Au NPs and small amounts of sample are required for the analysis [45],[46]. UV-vis spectrophotometers direct a light source through a sample and a detector on the opposite side the transmitted light is recorded. Typically, graphs of the data have the baseline at the bottom with the peaks pointing upward and they report wavelength in nanometers (nm) on the x-axis and absorbance (A) on the y-axis (no units). The transmittance represents how much light is absorbed at each wavelength and we are most interested in the highest peak (λmax) [47]. The intensity of light absorbed is directly proportional to the concentration of Au NPs in solution as obtained from beer lamberts law. (Eq. 3).

$$A = \varepsilon cl \qquad \text{Eq. (3)}$$

where A is the absorption of light at a specific wavelength, ε is the molar absorptivity and l is the length of the light path.

The size and shape of the NP can be estimated from the peak absorption wavelength whereby isotropic Au NPs only absorb in the visible spectrum (~ 520 nm) while anisotropic Au NPs have two absorption maxima's, one occurring in the visible spectrum around 520 nm and the other extending into the infra-red spectrum. Furthermore, an increase or decrease in Au NP yield can be quantitively determined by the change in absorption maxima of the measured Au NP colloids, while Au NP aggregation will lead to a disappearance of absorption bands.

For our experiments, a Thermo-Fisher scientific spectrophotometer (Evolution 220 UV-Visible spectrophotometer) was used to collect absorbance spectra for the as synthesized Au NPs. The absorbance measurements for the seed-mediated protocol were performed by scanning 3 mL of the

as-synthesized Au NPs at a wavelength of 200 – 1100 nm. Absorption measurement for the two-step sonochemical route was obtained by diluting 1 mL of Au NP colloid with 2 mL of water and scanning at wavelength between 275 nm – 500 nm, milli-Q water was used as the blank. For the optimized protocol, a mixture of glucose and water was used as the blank and 3 mL solution of the synthesized Au NPs was scanned at a wavelength between 400 – 800 nm.

For Iodometry experiments, 3 mL of the sonicated solution at 5 min intervals up to 30 mins were measured at a fixed absorbance of 350 nm.

3.3.2 FT-IR

Fourier transform infra-red (FT-IR) spectroscopy was performed to evaluate the molecules adsorbed on the Au NP surface responsible for the reduction of the Au precursor and capping of the Au NPs. This technique allows for the characterization of functional groups (OH, NH or CO) based on their characteristic absorption in the infra-red spectrum. The infra-red absorption frequency depends on the vibrational modes while the intensity depends on the energy transferred to the molecule [48]. FT-IR spectra of Au NP samples were collected by dropping colloids or solids on the sample holder and absorption measurements were obtained from wavelengths between 400 – 4000 nm. Pure glucose powders were used as reference for the absorption peaks. The pattern of the absorption spectrum is like a fingerprint that identifies the molecule, which lends itself to both quantitative and qualitative analysis.

3.3.3 SEM

Scanning electron images are useful to characterize the size and shape of the Au NPs. Images are obtained by images scanning the surface with a focused beam of electrons which interact with atoms in the sample, producing various signals that contain information about the surface topography and composition of the sample. For high resolution SEM samples, the Au colloids were dropped on TEM grids (Ni with lacy carbon) and allowed to dry under vacuum overnight before imaging. Solid samples were deposited on TEM grids using plastic spatulas to avoid contamination for both high- and low-resolution imaging. SEM-EDS point spectrums were taken from single

points of the obtained images. SEM is cheaper and faster than TEM and can provide size and compositions of the Au NPs.

CHAPTER 4 ARTICLE 1: SONOCHEMICAL SYNTHESIS OF GOLD POTATOES IN A ROSETTE CELL FOR APPLICATION IN DRUG DELIVERY SYSTEMS

Ndifreke Usen[a], Si Amar Dahoumane[a], Mamadi Diop[a,b], Xavier Banquy[c], Daria C. Boffito[a*]

[a]*Chemical Eng., Polytechnique Montréal, 2900 Edouard Montpetit Blvd, Montréal, H3T 1J4, QC, Canada*

[b] *Biomedical Eng., Université de Montréal, 2900 Edouard Montpetit Blvd, Montréal, H3T 1J4, QC, Canada*

[c]*Faculty of Pharmacy, Pavillon Jean Coutu local 4198, Université de Montréal, 2900, boul. Édouard-Montpetit, Montréal, H3T 1J4, QC, Canada.*

Corresponding author: daria-camilla.boffito@polymtl.ca

Submitted to Ultrasonic Sonochemistry in August 2021

This article represents the main results of the research project.

Abstract

We report the synthesis of gold nano- and micro-particles that relies on α-D-glucose ($C_6H_{12}O_6$) as the reducer and stabilizer in a Rosette cell under 20 kHz ultrasound irradiation. The chemical and physical effects of ultrasonic irradiation on the synthesis were investigated. The results showed that an optimum pH is required for the formation of insoluble Au (0) particles. Upon irradiation, low pH yielded gold nanoparticles while high pH resulted in microparticles. The Au surface capping by α-D-glucose hydroxyl and carbonyl groups was confirmed by Fourier transform infrared (FT-IR) spectroscopy. X-ray diffraction (XRD) analysis indicated that the Au particles crystallize within the face-centered-cubic (FCC) cell lattice. Moreover, continuous sonication reduced larger amounts of the Au precursor compared to the intermittent mode. Furthermore, tuning sonication time and mode influences the particle size and porosity as characterized by scanning and transmission electron microscopy. Our results shed a new light into the importance of the experimental and ultrasound parameters in obtaining gold particles of desired features through sonochemistry.

Keywords: Sonochemistry; Rosette cell; Gold nanoparticles; Porous particles; Anisotropic particles; Glucose

4.1 Introduction

Nanotechnology deals with the production, manipulation and use of materials ranging from 1-100 nanometers (nm). Nanoparticles can be manufactured with similar sizes and shapes to biomolecules; this makes them suitable for various applications in nanomedicine, such as targeted drug delivery, molecular imaging and biosensing [1–3].

Gold nanoparticles (Au NPs) are highly demanded for different applications in various fields, especially in nanomedicine [52][53]. For instance, Au NPs are among potential candidates to selectively attach to tumor cells through binding affinity [54] [7] Numerous approaches have been elaborated for the synthesis of Au NPs; however, only a few reports exist on the synthesis of gold microparticles (Au MPs) [56]. Microparticles are successful delivery vehicles capable of encapsulating/tethering interesting molecules to elicit efficacious and controlled release based on unique properties: particle size, shape, structure, entrapment efficiency, drug loading, porosity, targeting and release. The continuous manufacturing of Au MPs with controlled particle size is gaining attention based on concerns about the biodistribution and possible toxicity at the nanoscale [57].

Au NPs are known to change their color based on their size, shape, and surrounding medium; this is a chemo-physical property referred to as the surface plasmon resonance (SPR) making them suitable as thermal energy vehicles for the ablation of tumor cells [55]. Tiny Au nanospheres (Au NSs) display only a single SPR peak, occurring at a wavelength of ~520 nm [58]. On the other hand, Au nanorods (Au NRs) display two SPR bands, corresponding to the transversal (T) and longitudinal (L) modes [59], [60]. The first SPR peak (T mode) is located in the visible region, centered at ~520 nm, while the second SPR peak (L mode) can be easily tuned by varying the aspect ratio of the rods (length/width) to be located in the near-infrared region (NIR), suitable for deep penetration of light into biological tissues with applications in the photodynamic or photothermal therapy of cancer [61], [62]. Besides, the light scattering of Au NPs is exploited in surface-enhanced Raman spectroscopy (SERS) for cell labelling [63][64]. On the other hand, Au NRs have been shown to enhance fluorescence signals compared to Au NSs due to their SPR longitudinal mode [65]. Eustis and El-Sayed found that Au NRs are more suitable for imaging while hollow Au NPs and Au nano-shells are better as therapeutic agents [66].

Recently, biomolecules, especially simple and small sugars, such as glucose [67], starch [68], and sucrose [69], have gained attention as safe and eco-friendly reducing agents to promote the synthesis of Au NPs with 3-39 nm in size. Moreover, the use of a green stabilizer, such as glucose, in combination with ultrasound, can accelerate the NP formation while simultaneously controlling the particle size and shape [70], [71]. X-ray studies elucidating the reaction of Au(III) complexes with glucose show that a base, such as sodium hydroxide (NaOH), is required to hydrolyze chlorine atoms before the reduction of Au3+ can occur [72]. Sonochemistry, the application of ultrasound waves for the reduction of metal ions or complexes in solution, has been explored as a green process for the synthesis of size- and shape-controlled Au NPs. Compared to other chemical methods, ultrasound processes accelerate chemical reactions, reduce particle size, minimize the use of hazardous reagents and limit the generation of harmful by-products [73]. The sonochemical synthesis relies on the generation of radicals derived from acoustic cavitation, towards enhancing chemical reactions and the subsequent formation of novel nanomaterials [74]. While investigating the chemical effects of acoustic cavitation using a 20 kHz ultrasound processor operated at 500 W in order to quantify the production of reactive radicals, Laajimi et al. concluded that fewer radicals were produced at lower amplitudes (power) in the presence of small SiO2 particles [75].

The sonochemical synthesis of Au NPs is influenced by the synthesis and operating parameters as well as by the geometry of the vessel. The influence of ultrasonic power was explored by Garcia et al. using a 20 kHz processor whereby an increase in ultrasonic power decreased particle size and polydispersity. At a power of 60 W, the Au NP solution was violet with a decreased SPR intensity due to the nucleation and growth of large particles and increased polydispersity. Samples irradiated with powers of 120 W or 150 W produced ruby red suspensions with a lower polydispersity [34]. Similarly, Khani et al. observed that increased ultrasonic power reduced particle size and improved the crystallinity of Mn doped TiO2 photocatalyst [76]. At 40 kHz, glucose produced gold nanobelts; when glucose was substituted by cyclodextrin, only spherical NPs were obtained while longer irradiation times merged Au NPs to yield nanobelts.

In general, the conditions that provide the beneficial effects of sonochemistry in Au NP synthesis, such as reactor or ultrasound systems, are not widely examined in the literature [77]. Ultrasound frequencies from 20 kHz to 950 kHz have been explored for sonochemical synthesis purposes although higher frequencies require more power. Furthermore, the number

of radicals generated is larger at lower frequency. Radical generation is a chemical effect of acoustic cavitation. Radicals are generated when the instantaneous local pressure is negative in a liquid irradiated by ultrasound resulting from bubbles generated by dissolved gases [78]. For this reason, typical operating frequencies in the range of 20-40 kHz are employed in benchtop processors for NP synthesis. The physical and chemical effects of ultrasound irradiation arise from transient cavitation dominating at lower ultrasound frequency (20 kHz) [79]. Transient cavitation results in relatively more violent collapse of cavities followed by fragmentation, consequently generating new cavitation nuclei [80]. Reports show that ultrasound horns at low frequency contribute to an increase in radical production [81] while intermittent pulse sonication is favored due to a slower temperature rate increase from the resulting cavitation process, thereby avoiding undesired side-effects [82]. The main difference between sonochemistry and thermal processes resides in the collapse of bubbles rising from acoustic cavitation [83] leading to localized high temperatures and pressures which generate highly reactive species advantageous to nanomaterial fabrication [84]. In addition to the chemical effects owing to radical generation, particle size reduction and surface area increase derive from the physical effects of ultrasound irradiation, as depicted by Stucchi et al.; both features are critical for the adsorption of drug molecules [85]. Likewise, the use of a Rosette cell was found to be more effective in reducing the particle size of sodium-exchanged vermiculite due to the additional hydrodynamic cavitation [86]. Used to produce biodiesel under ultrasound irradiation, this reactor increased the transesterification yield by 90% when compared to a round-bottom glass flask; this geometry favors the hydrodynamic cavitation which usually occurs in small orifices, herein under the form of the reactor loops. Indeed, the loops would help faster dissipate the heat delivered by ultrasound, thus limiting the temperature rise and keeping more gas nuclei dissolved [87].

In this work, we describe a novel method for the sonochemical production of Au MPs and Au NPs in a Rosette cell reactor, whereby the ultrasound waves from the probe are propelled around the typical loops of this reactor. The synthesis method is simple and eco-friendly, it produces Au MPs and AuNPs passivated by hydroxyl and carbonyl functional groups, making them suitable for biomedical applications. This involves, first, the reduction of the Au precursor, followed by the stabilization and aggregation of colloidal NPs that occur in an alkaline medium containing α-D-glucose. Two different methods are utilized to produce Au

MPs and AuNPs. In a two-step sonochemical (1st) method, all reactants are added during the sonication to produce stable Au NPs while the seed-mediated sonochemical (2nd) method involves the pre-formation of Au nuclei which produce porous Au MPs of twinned gold nanospheres upon ultrasound irradiation. The seed-mediated route has proven to be suitable for the fabrication of Au MPs of controlled size as this remains poorly studied. Besides lowering the activation energy needed for metal reduction, our method enables the control over the growth conditions when renewable, cheap, eco-friendly and weak reducing agents, such as glucose, are exploited in nanoengineering.

4.2 Materials and Methods

4.2.1 Materials

Gold tetrachloride trihydrate ($HAuCl_4 \cdot 3H_2O$, 99%), α-D-glucose ($C_6H_{12}O_6$, 99%), and sodium hydroxide (NaOH, 99%) were purchased from Sigma Aldrich (St. Louis, MI, USA), potassium iodide (KI, 99%) was purchased from Sigma Life Sciences (Oakville, ON, Canada) and used as received. Deionized water (DIW) (18 MΩ, 4.3 μS/cm, Millipore) was the solvent.

4.2.2 Equipment

All Au NP synthesis experiments were carried out in a Rosette cell reactor (Figure S1) (Sonics and Materials, Newton, CT, USA).

A Rosette cooling cell is used instead of a conventional beaker to achieve higher mixing efficiency provided by unique flow patterns through the reactor's lateral loops (coils). During the sonication, the solution is circulated from the bottom to the top of the reaction vessel. Besides, the immersion in a cooling bath allows the exposure of a larger surface area of the reactor to the cooling medium, creating a more efficient heat exchange compared to a conventional beaker.

The ultrasound equipment (Sonics® & Materials, Inc., Newtown, CT, USA) included a 20 kHz Vibracell control panel operating at 130 W, a transducer (model CV18), fitted with a probe of 3 mm diameter tip (Figure 4-2). The ultrasound intensity was controlled by changing the amplitude. The power density of the ultrasound processor with the 3 mm probe was calibrated with a K type thermocouple. The probe and thermocouple were dipped into DIW, and the

temperature increase induced by sonication (for 9 min) was recorded to derive the power density for volumes of 10, 15 and 20 mL following the calorimetric method [88].

The experiments were carried out under either continuous or intermittent ultrasound irradiation. In the intermittent experiments, the ultrasounds were on for 30 s and off for 59 s. The probe was maintained at 1 cm from the bottom of the Rosette cell. The power density for the different experiments was calculated by dividing the total energy delivered (J) by the cumulative amount of time for which the probe was on and the volume of the medium. Besides, the energy absorbed by the solution was determined by potassium iodide (KI) dosimetry [89].

An isotemp bath circulator (6200 R28, Fischer scientific, Pittsburg, PA, USA) maintained a temperature of 25 ± 1 °C during the sonochemical synthesis. pH values during the experiments were measured using Orion Star A214 pH/Ise Bench Top Meter (Thermo Scientific) with a glass electrode.

4.2.3 Determination of sonochemical activity in the Rosette cell

Experiments were conducted in a Rosette reactor and were compared to their beaker counterparts of the same volume (30 mL), immersed in a thermostatic bath at 25 °C. Briefly, 1 mM potassium iodide (KI) was dissolved in 15 mL DIW. Ultrasound parameters optimized in the seed-mediated protocol were applied. The solutions were sampled after continuous or intermittent sonication for 30 min at regular intervals of 5 min. The $I3^-$ concentration is calculated using the Beer-Lambert law: $A = \varepsilon Cl$.

4.2.4 Seed-mediated sonochemical synthesis of Au MPs

For this experiment, α-D-glucose and NaOH were used to synthesize Au MPs. The effect of glucose concentration, pH, order of reagents' addition and ultrasound irradiation time on the Au MP formation was investigated through a series of experiments (Tables 4-1 and 4-2).

Table 4-1 Seed mediated sonochemical synthesis of Au MPs

$HAuCl_4$ (mM)	NaOH (mM)	$C_6H_{12}O_6$ (mM)	**pH**
12.6	38	9.9	5
12.6	63	19.9	7
12.6	115	39.9	12

Table 4-2 Parameters (mixing sequence, sonication mode and sonication time) varied during the seed-mediated synthesis of Au MPs.

Sample	Mixing Sequence	Sonication Mode	Time (min)	λ_{max} (nm)	Yield Au^{3+}	A (a.u.)	Au^{3+} (mg mL^{-1})
NG-35-I	NaOH→$C_6H_{12}O_6$	30 s on: 59 s off	35	276	81	0.2053	0.0605
GN-30-I	$C_6H_{12}O_6$→NaOH	30 s on: 59 s off	30	274	80	0.203	0.0601
GN-30-I	$C_6H_{12}O_6$→NaOH	30 s on: 59 s off	30	276	80	0.2014	0.0598
NG-40-I	NaOH→$C_6H_{12}O_6$	30 s on: 59 s off	40	278	78	0.1931	0.0582
GN-40-I	$C_6H_{12}O_6$→NaOH	30 s on: 59 s off	40	276	77	0.19	0.0576
NG-30-C	NaOH→$C_6H_{12}O_6$	Continuous	30	272	75	0.1829	0.0562
NG-40-I	NaOH→$C_6H_{12}O_6$	30 s on: 59 s off	40	276	73	0.1751	0.0547
NG-40-C	NaOH→$C_6H_{12}O_6$	Continuous	40	276	67	0.1511	0.0501
NG-30-I	NaOH→$C_6H_{12}O_6$	30 s on: 59 s off	30	276	65	0.1431	0.0485
GN-30-C	$C_6H_{12}O_6$→NaOH	Continuous	30	272	63	0.0149	0.0476
NG-30-C	NaOH→$C_6H_{12}O_6$	Continuous	30	276	59	0.1212	0.0443
GN-40-C	$C_6H_{12}O_6$→NaOH	Continuous	40	274	59	0.1209	0.0442

Initially, the seed solution was prepared by mixing 10 mL aqueous solutions of 12.6 mM $HAuCl_4$ with NaOH at 38 mM (pH 5), 63 mM (pH 7) and 115 mM (pH 12). Next, growth solutions containing 5 mL aqueous solutions of 12.6 mM $HAuCl_4$ mixed with $C_6H_{12}O_6$ concentrations at 9.9 mM, 19.9 mM, and 39.9 mM at pH 2 were prepared; the solutions were yellow in color. The seed solution turned from yellow to transparent within 30 s with a color change rate depending on the added amount of NaOH. Mixing HAuCl4 with NaOH produces gold hydroxide ($Au(OH)_4^-$ aq) and sodium chloride (NaCl aq). Then, the seed solution ($HAuCl_4$ and NaOH) and growth solution ($HAuCl_4$ and $C_6H_{12}O_6$) were mixed to obtain final pH values of 5, 7 and 12 (Figure 4-1). Following the combination of the seed and growth solutions, probe sonication was applied at a power output of 20 ± 1 W and ultrasound power density of 1.3 W mL-1 for 30 min resulting in the production of anisotropic Au MPs at pH 7 and porous Au MPs at pH 12 with the porosity and size depending on the mixing sequence and sonication mode.

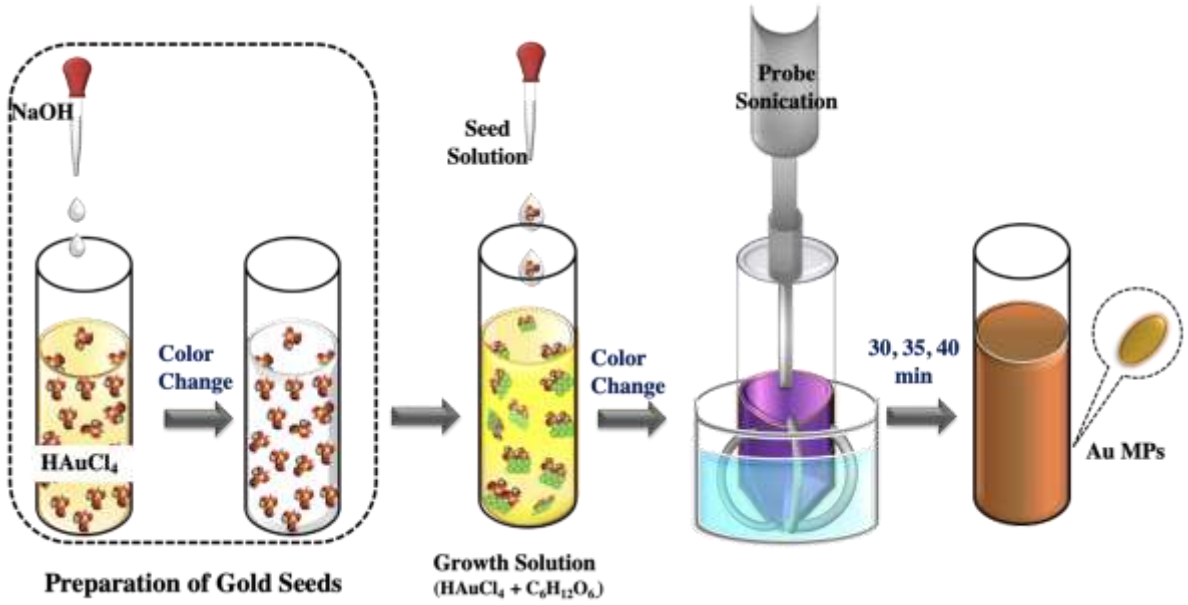

Figure 4-1 Illustration of the synthesis of porous Au MP at pH 12 and anisotropic Au MPs after aging at pH 5 and 7 via seed mediated sonochemical process.

For the experimental design (Table 4-2), we focused on repeating our initial results obtained at pH 12 from the simple 32 factorial design (Table 4-1). This experimental design aimed at

screening the operating and synthesis parameters that influenced the formation of precipitated porous Au MPs. The effect of mixing sequence (NaOH first, then $C_6H_{12}O_6$, and vice-versa), sonication time (30 min and 40 min with a mid-point at 35 min) and sonication mode (intermittent vs. continuous) on the particle size and morphology were explored at a constant power output of 20 ± 1 W corresponding to an ultrasound power density of 1.3 W mL-1. Mixing the growth and seed solutions yielded a violet solution which, after sonication, became a clear suspension with dark particles that precipitated at the bottom of the Rosette cell. For each treatment, the probe position was maintained at ~1 cm from the bottom of the reactor. Furthermore, a total energy consumption of ~49,000 J was recorded for all the experimental runs. On the other hand, the difference in recorded total energy from the processor during intermittent vs. continuous sonication was negligible.

4.2.5 Two-step sonochemical synthesis of Au NPs

Au NPs were synthesized following a two-step sonochemical process (Table 4-3).

Table 4-3 Two-step sonochemical synthesis of porous Au NPs

Sample	$HAuCl_4$ (mM)	$C_6H_{12}O_6$ (mM)	NaOH (mM)	Energy (W mL^{-1})	pH	Outcome
10 mL solution (A)	4	200	0	1.0	2	No reduction
20 mL solution (B)	2	100	0	0.5	2	Au^{3+} reduction
15 mL solution (C)	8	200	6.6	0.6	9	Au(0)
25 mL solution (Exc.)	8	200	12	0.4	12	Au(0)

For this experiment, we initially followed the work by Zhang et al. [90] who used a 40 kHz ultrasonic processor to synthesize gold nanobelts (Au NBs) using α-D-glucose as both the reducing and capping agents. During the first step, the probe sonication was continuously applied to aqueous solution-A containing 2 mM $HAuCl_4$ and 100 mM $C_6H_{12}O_6$ inside a Rosette cell reactor kept in a thermostatic water bath at 25 ± 1 °C. A digital thermometer in the reaction vessel during the sonication process recorded a temperature rise of 5 ± 1 °C. We observed no changes in the color or absorbance of this solution implying that the synthesis result/outcome

did not lead to the reduction of the Au precursor. Therefore, we decided to increase the solvent volume thereby decreasing the concentrations of both the Au precursor and reducing agent. Solution-B was prepared by maintaining the same molar ratio of the reagents and ultrasound parameters as in solution-A; however, DIW volume was increased to 20 mL. The change in solvent volume led to a positive outcome whereby we observed a slight reduction in peak intensity which correlates with a slight reduction of the Au precursor (Au^{3+}) after sonication for 90 min. This process concluded the first step of the experiment. The power output was 10 ± 1 W for both solutions, as recorded by the digital processor. However, the power density at an amplitude of 68% was 1.0 W mL^{-1} for solution-A and 0.5 W mL^{-1} for solution-B.

After 24 h storage at 4 °C, 5 mL of solution-A were mixed with 5 mL of solution-B at pH 2, followed by direct probe sonication with a power density of 1.1 W mL^{-1}. The solution remained yellow and no color change or UV-Vis absorbance peak was observed after 30 min in that case. For solution-C, 10 mM NaOH were added dropwise into the mixture of solution-A and solution-B undergoing ultrasonic irradiation with a power density of 0.4 W mL^{-1} producing a violet color at a corresponding pH of 9. A neat SPR peak at 563 nm measured by UV-Vis confirmed the formation of Au NPs. The change in color occurring during the addition of NaOH under continuous irradiation signifies a positive outcome whereby the Au precursor is completely reduced from an oxidation state of Au^{3+} to Au (0). Adding excess NaOH (solution Exc.) with a power density of 0.6 W mL^{-1} changed the color of the suspension from violet to blue at pH 12, and the intensity of the corresponding UV-Vis peak decreased. The solvent volume, reaction time and power delivered from the probe resulted in the formation of Au NPs at pH 9 and Au MPs at pH 12 (Figure 4-3).

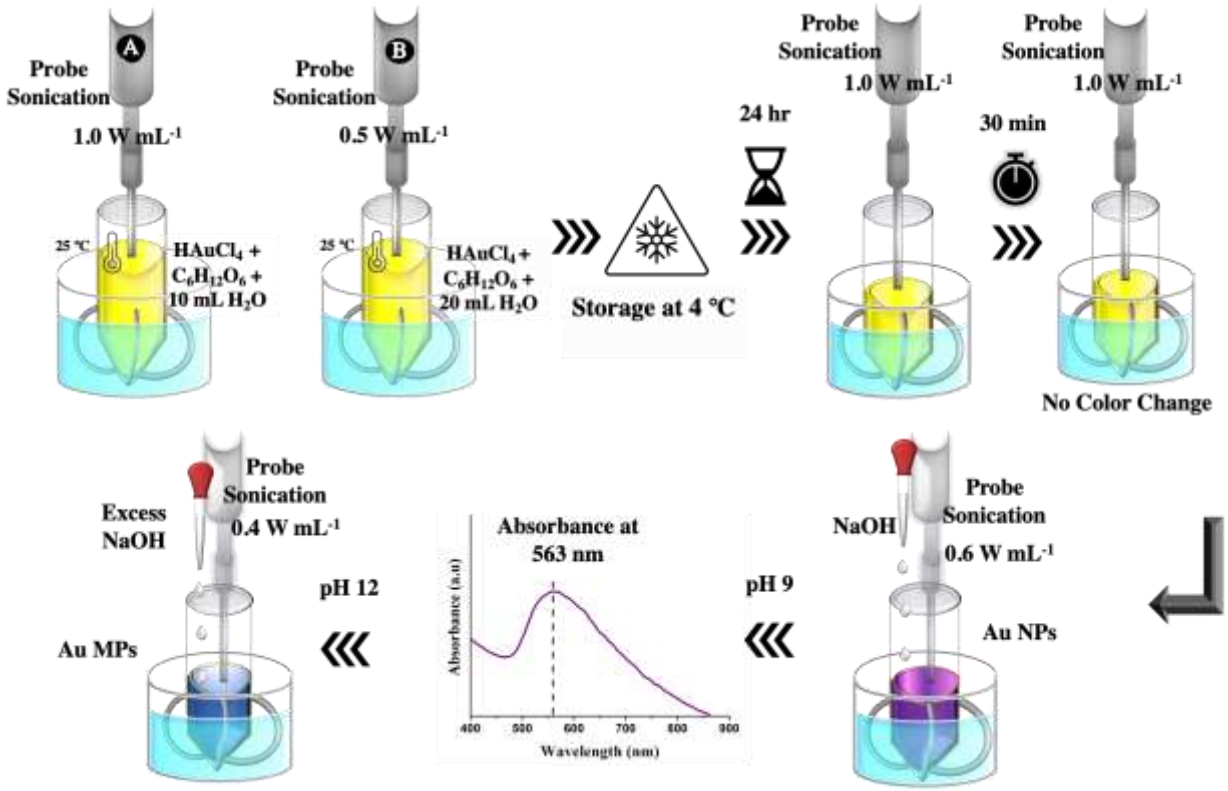

Figure 4-2 Synthesis of porous Au NPs via a two-step sonochemical process.

4.3 Characterization of gold nanoparticles

The Au ions and Au NPs were characterized using UV-Vis absorption spectroscopy (Thermo Scientific Evolution 220 UV-Vis spectrophotometer, Madison, WI, USA) in quartz cuvettes with DIW as the blank. The morphology and the chemical nature of the produced NPs were studied using scanning electron microscope (TM3030Plus Hitachi Tabletop Microscope, Toronto, ON, CA; JOEL JSM-7600F, Tokyo, Japan) and transmission electron microscope (JOEL 2100F, Tokyo, Japan). SEM-EDX images were performed at 15 keV with solid samples cast on carbon grids. The adsorption of glucose moieties on the surface of the as-synthesized Au particles was confirmed using Fourier transform infrared spectroscopy (Spectrum 65, Perkin Elmer, Woodsbridge, ON, CA).

4.4 Results and Discussion

4.4.1 Effect of $HAuCl_4$ concentration under continuous ultrasonic irradiation

In the two step protocol, we modified the operating procedure by using a 20 kHz ultrasound processor instead of 40 kHz and the $HAuCl_4$ precursor was diluted 100 times when compared to the one used by Zhang et al. [43]. In our case, a mixture of $C_6H_{12}O_6$ at fixed HAuCl4 concentration did not yield Au NPs in the absence of the NaOH-containing seed solution. The addition of NaOH during the sonication process resulted in colloidal Au NPs after aging; similar results were obtained via the seed mediated synthesis route.

In the two-step protocol, when aqueous Au(III) precursor solutions containing α-D-glucose were sonicated in a NaOH-free medium for 90 min, the reduction of Au(III) to Au(0) did not occur. For instance, solution A, containing 4 mM $HAuCl_4$ showed no visible color change and no SPR peak (Figure 4-4A). However, a decrease in the Au(III) absorbance intensity occurred in solution-B containing 2 mM $HAuCl_4$ after 90 min of direct sonication; this might be due to the hydrolysis of $HAuCl_4$ (Figure 4-4B). The reduction in peak intensity for the diluted solution-B can be attributed to the thermal dissociation of water molecules producing H• and OH• which participate in the subtraction of a proton from the Au precursor. In addition, methyl groups resulting from the thermal decomposition of glucose molecules in the reaction medium could trigger the removal of a proton thereby reducing the Au precursor concentration [44].

Solvent volume is an important parameter to establish the sonochemical efficiency of irradiated solutions. This is reflected in the reduced peak intensity observed for the 20 mL solution (Figure 4-4B) which remains unaffected in the 10 mL solution (Figure 4-4A) even after prolonged sonication. In a 37 kHz ultrasound bath, the degradation of amoxicillin by waste sludge catalyst was dependent on its concentration [45]. Similar to our experiments, a decrease in absorbance peak was only observed for solutions with lower Au precursor concentrations at larger volume. Since no absorbance change was observed after 90 min in the concentrated solution (10 mL), the dilution of the solution allows an increase in energy dissipation across the system aiding in the reduction of the gold precursor ($HAuCl_4$).

Mixing 5 mL of solution-A with 5 mL of solution-B under continuous sonication caused no visible changes to the color of the solution nor to the absorbance spectra. However, increasing the pH from

2 to 9 by adding NaOH turned the solution color from yellow to violet accompanied by the appearance of an SPR peak at 556 nm indicating the formation of colloidal Au NPs (Figure 4-4C). Consequently, the features of the Au NPs evolved dramatically whereby at pH 9 three-dimensional (3-D) Au NPs are formed (Figure 4-4D). Excess of added NaOH under sonication precipitated Au MPs at pH 12. This resulted in the disappearance of the SPR peak observed at 563 nm and a color change from violet to blue (Figure 4-4E) which became clear a day later owing to the appearance of Au precipitates at the bottom of the Rosette cell. Previous studies in a 50 kHz ultrasound bath using electron spin trapping technique to determine the radicals formed during ultrasonication showed that, at low concentrations of non-volatile solutes (e.g., $C_6H_{12}O_6$), H• and OH• are produced because of water sonolysis. On the other hand, solute pyrolysis leads to the formation of $CH_3^{\bullet}$ due to its thermal decomposition at sufficiently high concentrations [44]. In our case, continuous ultrasonication and high pH disrupted the stabilizing properties of glucose resulting in the aggregation of Au NPs and the subsequent formation of Au MPs.

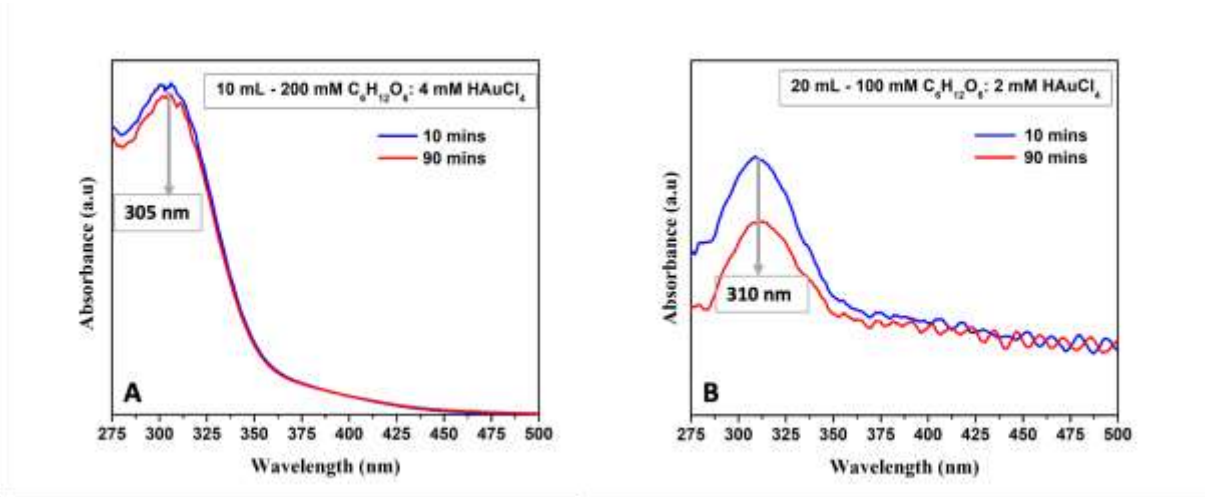

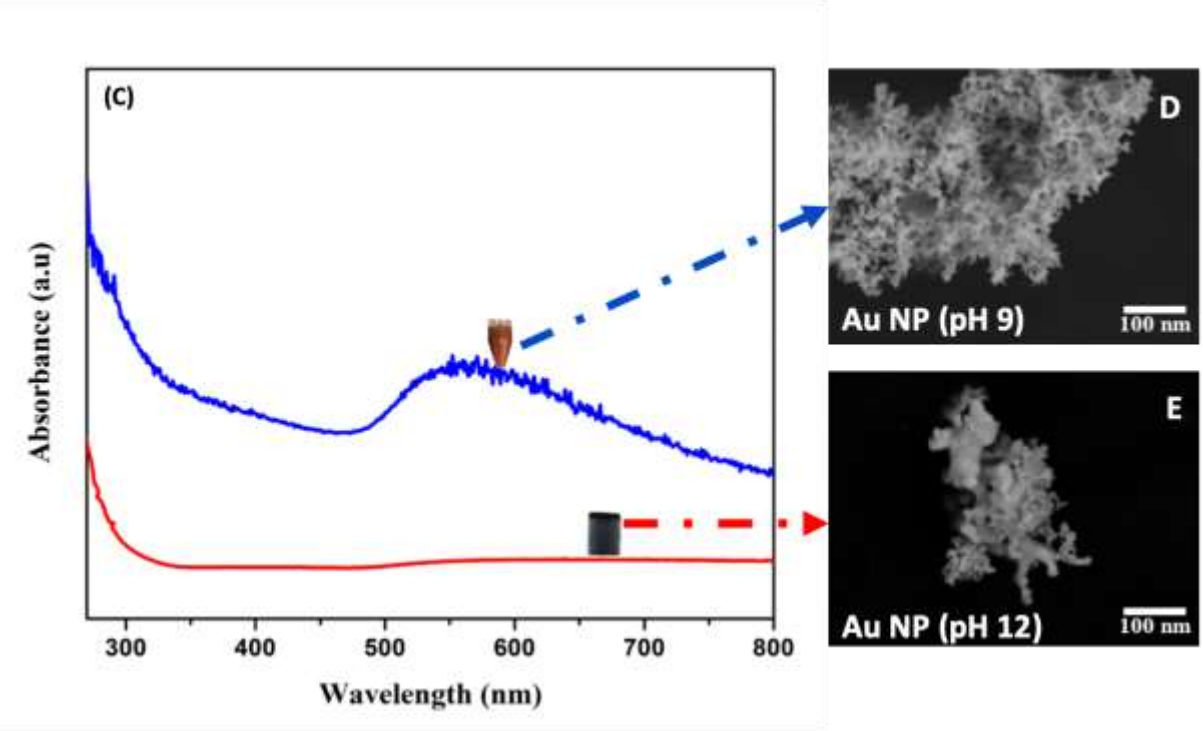

Figure 4-3 UV-Vis absorption spectra of continuously sonicated solutions of Au NPs: (A) 4mM $HAuCl_4$ and 200 mM α-D-glucose (B) 2 mM $HAuCl_4$ and 100 mM α-D-glucose, (C) UV-Vis absorption spectra of Au NPs synthesized via the two-step sonochemical method with addition of NaOH (D) SEM of Au NPs synthesized at pH 9; and (E) Au NPs synthesized at pH 12.

4.4.2 Effect of $C_6H_{12}O_6$ concentration under continuous ultrasonic irradiation

In the two-step synthesis protocol, the effect of $C_6H_{12}O_6$ concentration on the ultrasonic-mediated reduction of $HAuCl_4$ in NaOH-free reaction medium was investigated. Initially, the effect of glucose was not evident at low solvent volume. However, increased solvent volumes at 0.5 W mL-1 after 90 min of ultrasonic irradiation resulted in a decrease in the peak absorbance intensity for the solution containing 2 mM $HAuCl_4$ mixed with 100 mM $C_6H_{12}O_6$. This is ascribed to the chemical effect of the ultrasonic irradiation whereby the thermal dissociation of water and decomposition of glucose from cavitation lead to the production of OH• and H•, which take part in the reduction of the Au precursor. This is in good agreement with published data. For instance, Kondo et al. explored the radical formation in a 50 kHz ultrasound bath in aqueous solutions using a spin trapping method and showed that glucose concentrations above 0.2 M produced reducing $CH_3^{\bullet}$ due to pyrolysis [44]. Using a 200 kHz ultrasonic generator, Okitsu et al. evidenced that $CH_3^{\bullet}$ rather than aldehydes were responsible for the reduction of the Au precursor in an inert atmosphere [46]. Accordingly, it was reported that ultrasound frequency between 20-80 kHz can oxidize carbohydrates, such as glucose, in the presence of oxidants [47]. These results indicate that $C_6H_{12}O_6$, by itself, does not reduce Au ions under low frequency ultrasound. Furthermore, control experiments using heat did not result in Au NP formation.

Via the seed-mediated protocol, for a $HAuCl_4$ concentration of 12.6 mM and in the absence of NaOH, increasing $C_6H_{12}O_6$ concentration of 10-40 mM did not bring changes to the reaction mixture, indicating that a suitable activation energy was required before glucose could reduce the Au ions in solution. $C_6H_{12}O_6$ does not seem to possess any reducing property by itself as no significant reduction of $HAuCl_4$ was observed in the experiments at pH values below 7 while there is a possibility that it decomposes at higher pH under ultrasonic irradiation. El'piner and Sinclair described the decomposition of glucose in an alkaline medium under heat as a thermal effect comparable to the ultrasonic effect. The decomposition products resulting from thermal and ultrasonic processes had absorption maxima in the UV range [48].

Although a visible color change in the solution above pH 7 was noticed, no SPR peak was initially recorded. However, after aging, there was a visible SPR peak that red-shifted and increased in intensity with increasing glucose concentration, suggesting a possible synergy between glucose

reduction and pH of the medium (Figure 4-5). At 10 mM $C_6H_{12}O_6$, SEM shows anisotropic shapes for the suspension (Figure 4-5A) and the precipitate (Figure 4-5B) with corresponding EDS (Figure S2) while, at 20 mM $C_6H_{12}O_6$ (Figure 4-5C) and 40 mM $C_6H_{12}O_6$ (Figure 4-5D), it displays precipitated and agglomerated Au NPs that have lost the anisotropic structures observed at lower $C_6H_{12}O_6$ concentrations. EDS analysis confirms that the agglomerated Au NPs are chemically composed of gold (Figures S3 and S4).

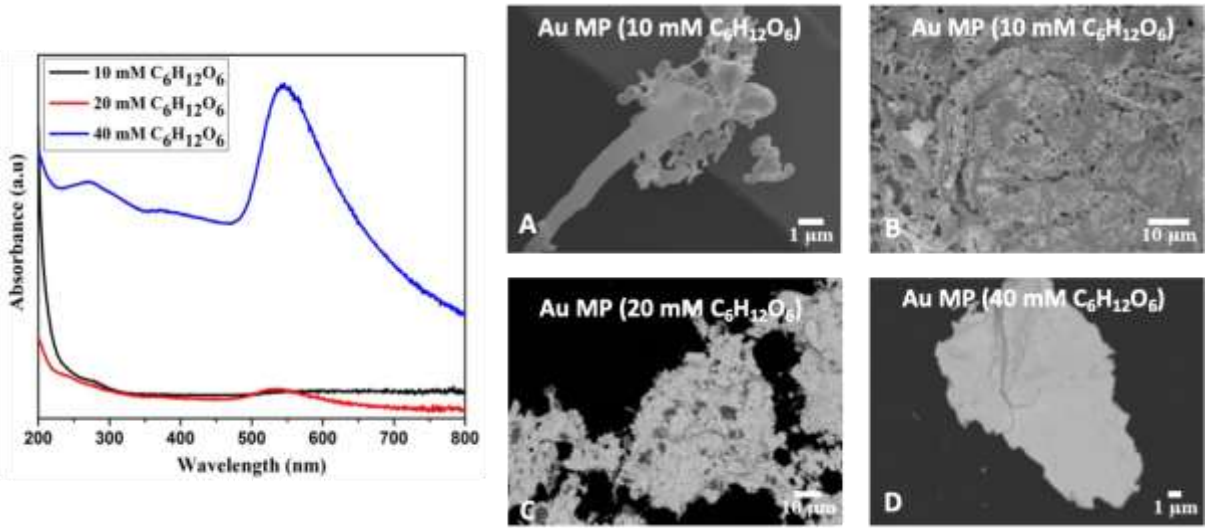

Figure 4-4 UV-Vis spectra and corresponding SEM of Au MPs formed under continuous ultrasound irradiation at pH 7 and (A&B) 10 mM $C_6H_{12}O_6$ concentration (C) 20 mM $C_6H_{12}O_6$ concentration (D) 40 mM $C_6H_{12}O_6$ concentration.

The efficiency of $C_6H_{12}O_6$ to generate reducing $CH_3^{\bullet}$ towards Au reduction and to act as a capping agent was verified in a separate experiment in an aqueous solution containing 200 mM $C_6H_{12}O_6$, 7.5 mM NaOH and 2 mM $HAuCl_4$. This experiment, designed with optimized concentrations of precursor and reducing agent, was conducted under continuous ultrasonic irradiation and compared to a conventional chemical synthesis route (Figure 4-6A). Evidently, the combination of high $C_6H_{12}O_6$ and low Au precursor concentrations produced significantly stable Au NPs (up to 1 month

at room temperature). It is noteworthy that these sets of experiments produced stable Au NPs with or without ultrasound at pH 7 and a low Au precursor. In this respect, there was a significant difference between the observed colors and recorded absorption spectra of the ultrasonic irradiated solution vs. the conventional synthesis (Figure 4-6A). The Au colloids produced via the chemical synthesis route had a red color with an SPR maximum located at 520 nm for the synthesis without heat (Ca) which red-shifted to 527 nm when heating was applied (Cb). On the other hand, Au colloids produced when NaOH was added during ultrasound irradiation (USa) had a violet color and an SPR maximum located at 532 nm which decreased in intensity when the reagents were pre-mixed prior to ultrasound irradiation (USb). These results corroborate our initial deduction that a molar ratio of Au precursor to $C_6H_{12}O_6$ (1:50), high solution volume and pH values between 7 and 9 are required to reduce and stabilize Au NPs when working at a low ultrasonic frequency (20 kHz). As $C_6H_{12}O_6$ is a weak reducing agent, low frequency ultrasound (20 kHz) requires longer sonication times to oxidize $C_6H_{12}O_6$ and generate $CH_3^{\bullet}$ that reduce the Au precursor. The NaOH addition during the ultrasonic treatment resulted in a slightly red-shifted SPR peak indicating an increase in NP size. When the reagents were mixed prior to ultrasound irradiation, the SPR peak had a weak absorbance and a broad peak indicating polydispersity and agglomeration. Adding NaOH under either ultrasound irradiation or stirring improved the stability of the formed Au NPs compared to samples where NaOH had been previously added; this was based on visual observation of samples stored at 4 °C for 1 week.

Glucose capping of Au NPs was confirmed using FTIR (Figure 4-6B). FT-IR measurements for Au MPS and Au NPs samples showed the presence of a polar covalent bond involving carbon and oxygen, ascribed to the glucose molecule. The strong absorption band of the –OH group observed at 3320 cm^{-1} was attributed to O-H stretching of intermolecular bonding of alcohol stemming from adsorbed OH groups on the surface of Au particles. The characteristic C=O group at 1636 cm^{-1} was attributed to the formation of an acetal group from the oxidation of the anomeric carbon of $C_6H_{12}O_6$ molecules. The absorption bands at 1030 cm^{-1} (solid $C_6H_{12}O_6$) and 1089 cm^{-1} (Au MPs) were attributed to the C-O stretch from the oxidized primary alcohol group of $C_6H_{12}O_6$.

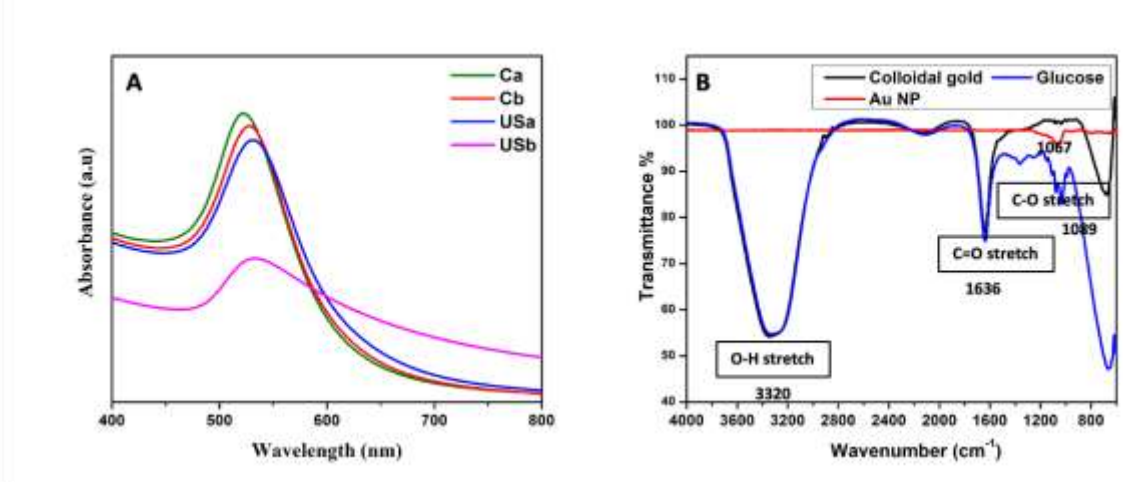

Figure 4-5 (A) Comparative UV-Vis study of Au NPs synthesized via different routes (Conventional and US) [Ca = Conventional synthesis with 75 mM NaOH added during stirring at 40 °C; Cb = Conventional synthesis with 75 mM NaOH added before stirring at 40 °C; USa = Ultrasound-assisted synthesis with 75 mM NaOH added under irradiation at 20°C; USb = Ultrasound-assisted synthesis with 75 mM NaOH before irradiation at 20°C; (B) FT-IR analysis of Au NPs with glucose as a capping agent synthesized at pH 7

4.4.3 Effect of pH

In the present study, NaOH was the only contributing factor that could affect the pH of the reaction medium. The addition of $C_6H_{12}O_6$ to Au3+ stock solution did not affect its pH 2 or color; besides, there was no impact on its UV-Vis absorption features. The addition of NaOH hydrolyzes HAuCl4 causing changes to the pH by substituting the Cl− groups with OH− groups, as follows (Eq. 4) [72]:

$AuCl_4^- + 4\ OH^- \rightarrow Au(OH)_4^- + 4\ Cl^-$ (Eq.4)

Our findings corroborate previous reports that highlight the critical role played by NaOH in the formation of Au NPs. At pH 12, a mixture of 12.6 mM $HAuCl_4$ and 40 mM $C_6H_{12}O_6$ produced a violet suspension prior to ultrasonic irradiation that evolved to brown after the irradiation due to the destabilization of the suspension through ultrasound mechanochemical effects. This further implies that there is an optimal pH required for the formation of stable Au NPs using α-D-glucose as the reducing and capping agent at 20 kHz (Eq. 5).

$Au(OH)_4^- + C_6H_{12}O_6 \rightarrow Au_{colloid}$ (Eq. 5)

Increasing the NaOH amount dramatically impacted the morphology of the obtained Au NPs. At pH 5, the Au NPs were one-dimensional nanowires mixed with thin plates (Figure 4-7A), analysis of the particles confirmed the presence of Au and carbon which was attributed to the grid used to support the dried suspension during analysis (Figure S5). Increasing the pH to 7, resulted in spherical Au MPs that where crosslinked (Figure 4-7B) and further increase to pH 12 resulted in the agglomeration of the produced Au NPs into ellipsoidal microstructures (Figure 4-7C). EDS analysis confirmed the agglomerated Au MPs are chemically composed of Au (Figure S6). Overall, the Au NP formation and stability can be tuned by optimizing the pH of the solution. In the synthesis of gold nanobelts, Zhang et al. did not change the pH, however we found that adding NaOH created a suitable environment for the formation of Au NPs and, consequently, the evolution of their morphology and optical properties.

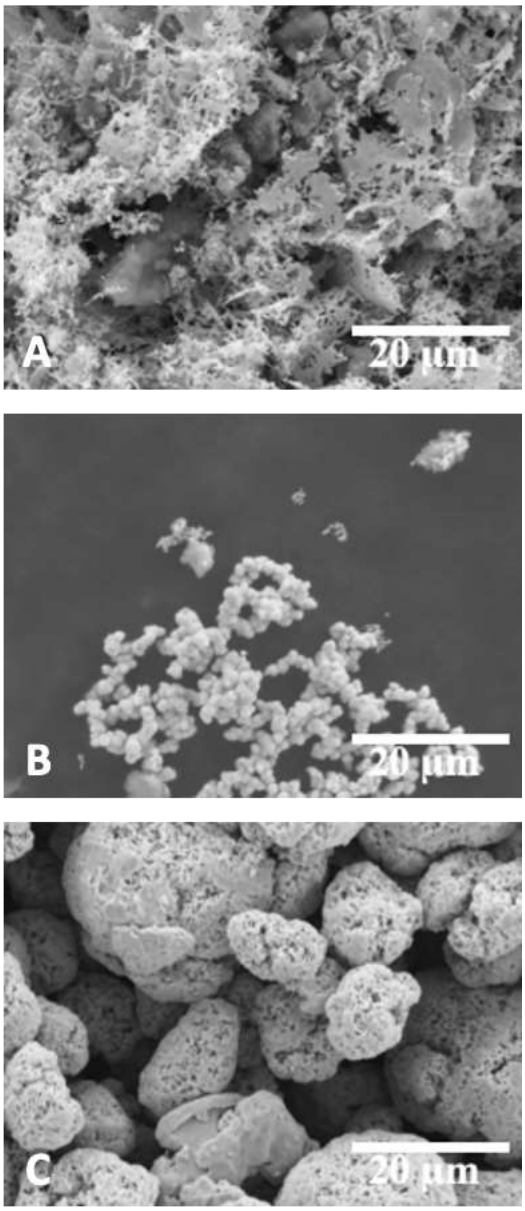

Figure 4-6 SEM micrographs of sonochemically produced Au NPs at pH 5(A); pH 7(B); and Au MPs at pH 12 (C).

4.4.4 Effect of ultrasound operating parameters

Building on the results of the seed-mediated procedure, the process and synthesis parameters were screened to determine their effects on formed Au particles. Specifically, the sequence of the growth solution (aqueous solution of glucose and Au precursor at pH 2) and seed solution (aqueous solution containing NaOH and Au precursor at pH 12) were varied, reaction times were set at 30, 35 and 40 min, and sonication mode was either continuous or intermittent to let the mixture cool (30 s on / 59 s off). The probe position was maintained at 1 cm from the bottom of the Rosette vessel while the acoustic intensity, as obtained from calorimetry, was 1.3 W mL^{-1}. For the experimental runs, the power output as obtained from the processor was 21 ± 1 W at 100% amplitude. During ultrasonic irradiation, the acoustic cavitation gives rise to $OH^{\bullet}$ and $CH_3^{\bullet}$ owing to water sonolysis and glucose pyrolysis, respectively. Acoustic mixing arises from changes in pressure and temperature in the liquid medium, leading to uniform shear rates and improved chemical reaction rates [84]. According to Wood et al., pulsed wave ultrasound increases the sonochemical active region, the amount of sonochemistry and associated degassing [81]. The concentration of unreduced Au precursor based on absorption intensity at 275 nm is lower in the case of continuous sonication mode, indicating a significant effect on the overall Au conversion at 30, 35 and 40 min, irrespective of reagent addition method (Figure S2). Cubilana et al. evaluated the effect of ultrasound power on the Au NP concentration and observed that increasing intensity of the UV-Vis absorption spectra correlates with an increase in Au NP concentration [91]. Based on our results, the peak intensity at 275 nm is higher for intermittent sonication compared to its continuous analog; this difference is correlated to the highest efficiency of continuous sonication towards the reduction of Au (III) into Au(0) (Figure 4-8A).

From a crystallographic point-of-view, the sonication mode, intermittent vs. continuous, had no impact. In fact, the XRD peaks of the synthesized Au NPs could be indexed to the face-centered cubic (fcc) cell lattice (JCPDS: 04-0784) of metallic gold. XRD analysis revealed four dominant peaks corresponding to (111), (200), (220) and (311) planes observed at angles located between 30° to 80° (Figure 4-8B) corresponding to the Bragg reflections obtained for metallic gold fcc crystal structure. Furthermore, the Au NPs crystallite size, calculated using Scherrer equation, were determined to be 16.4 nm and 17.8 nm for intermittent and continuously sonicated Au NPs, respectively, regardless of the sonication time, indicating that both Au NP populations are

polycrystalline. The Au (111) plane which is the dominant peak is identified as the most stable structure for the preferential adsorption of sulfur and nitrogen functional groups, making the as-synthesized Au NPs suitable for biomolecule attachment [92]. Similarly, Au NBs produced by Zhang et al. were preferentially grown along the (111) direction based on analysis of selected area electron diffraction (SAED) patterns [90].

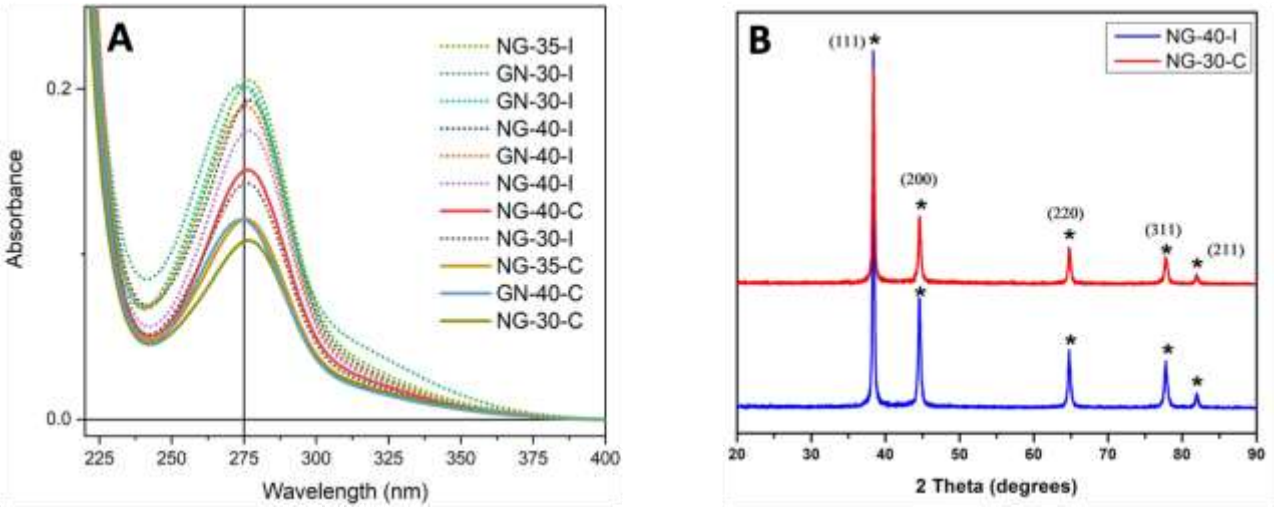

Figure 4-7 (A) UV-Vis absorption spectra for Intermittent (I) and continuous (C) pulse irradiating $AuCl_4$-OH; (B) X-ray diffraction pattern of polycrystalline fcc Au NPs.

The effect of sonication time was evident from SEM analysis of the Au MPs. When Au NPs prepared by the seed-mediated protocol were sonicated for 30, 35 and 40 min, porous Au MPs were obtained, as observed from TEM (Figure S3). The pore size is equivalent to 200 nm and the internal structure shows protruding Au particles layered on preceding particles. At 40 min, large porous particles are formed while 30 min sonication produced smaller potato-shaped structures (Figure 4-9). From high- and low-resolution SEM micrographs obtained using a back scatter detector (BSE), 30 min sonication produced microporous Au particles with more pore openings compared to samples subjected to 40 min sonication. The characterization of the microstructure using high resolution SEM shows that intermittent sonication produced layered particles with wider diameter openings for the agglomerated particles while particles with smooth surface and smaller diameter openings were obtained via the continuous sonication (Figure 4-10).

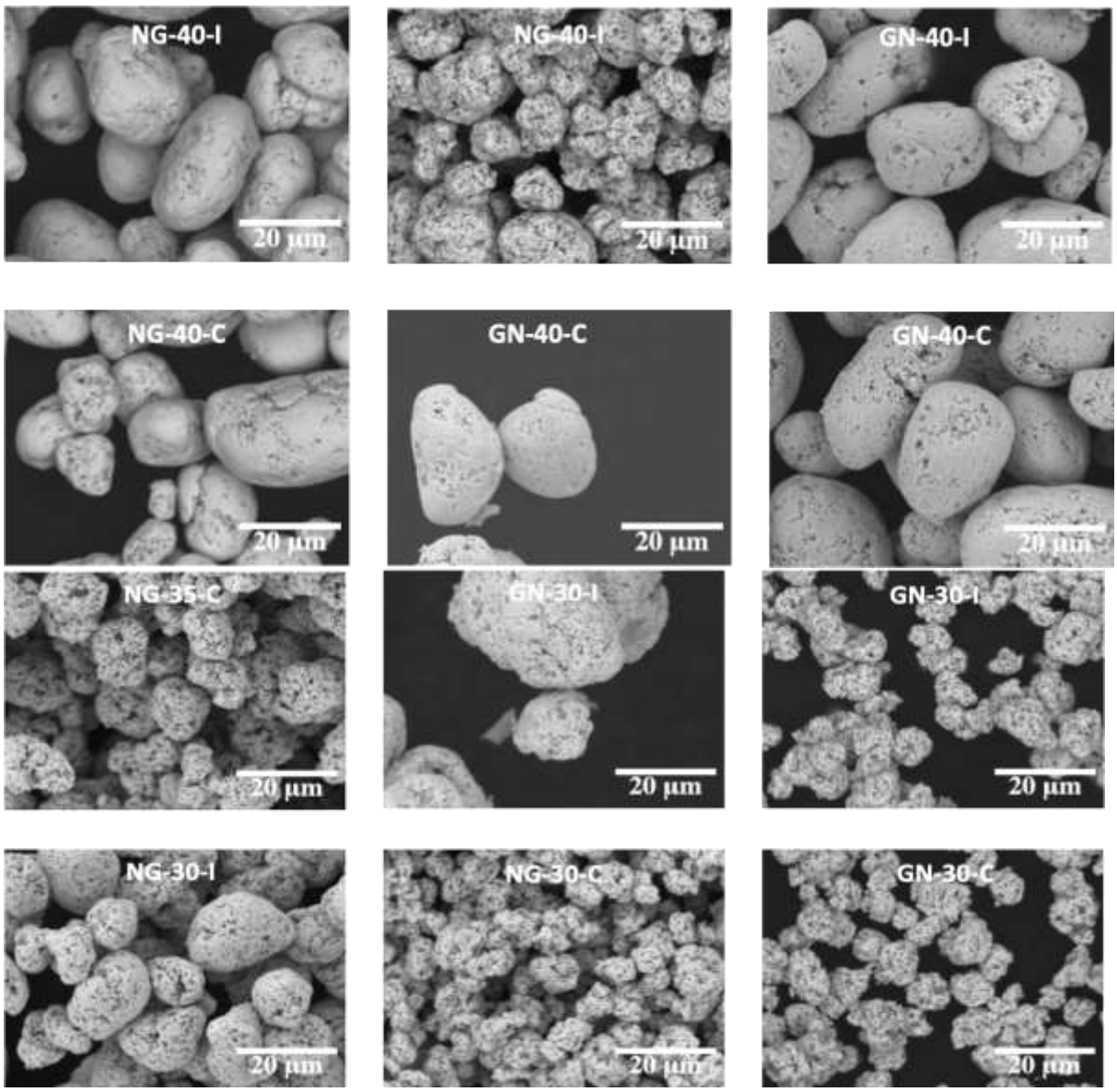

Figure 4-8 SEM micrographs of Au MPs obtained from the seed-mediated protocol; GN (Glucose added to NaOH-contain Au solution), NG (NaOH added to Glucose-containing Au solution); 30, 35 and 40 min (sonication time); C and I (Continuous or Intermittent pulse sonication mode).

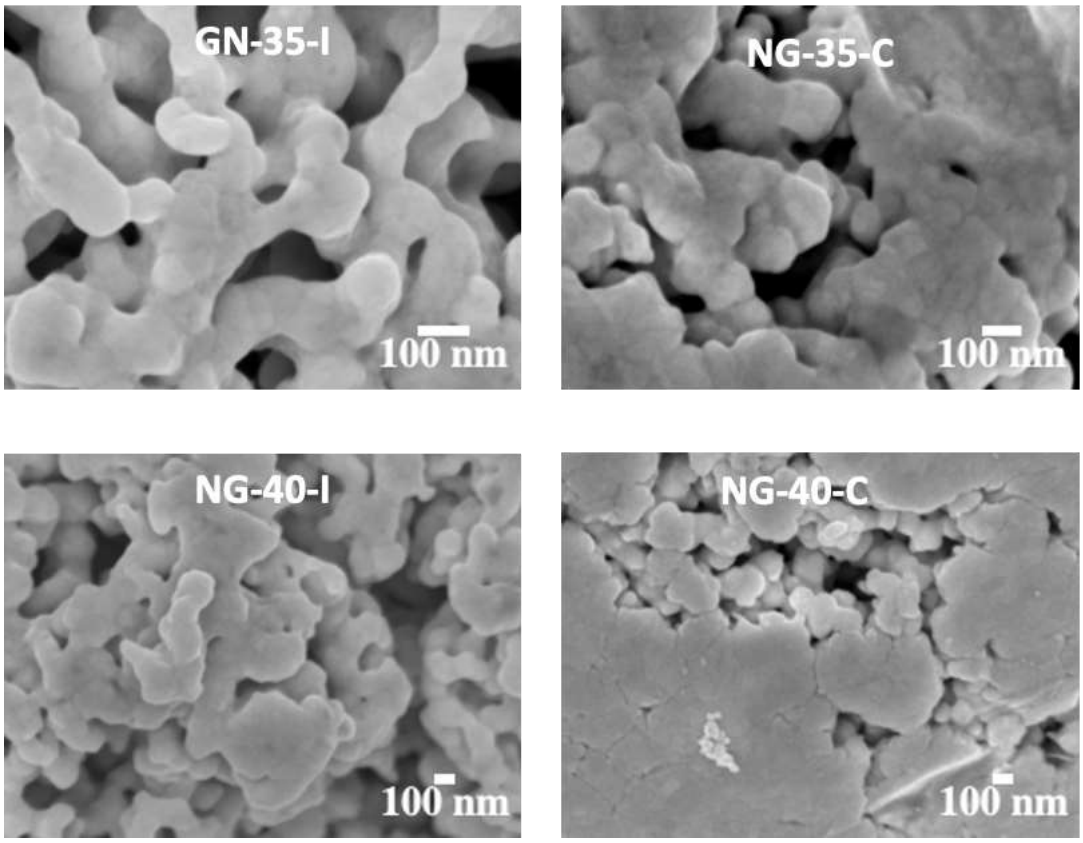

Figure 4-9 FEG-SEM micrographs of Au MPs obtained from the seed-mediated protocol; effect of sonication mode at 35 and 40 min. GN (Glucose added to NaOH-containing Au solution), NG (NaOH added to Glucose-containing Au solution); 30, 35 and 40 min (sonication time); C and I (Continuous or Intermittent pulse sonication mode).

4.4.4.1 Chemical effect of ultrasound on radical generation

When 1 mM potassium iodide (KI) is sonicated, the generated reactive radicals oxidize the iodide ion (I^-) to give iodine (I_2) (Eq. 6 & 7). This I_2 reacts with the excess iodide ion (I^-) to form tri-iodide ion (I_3^-) (Eq. 8-10). The amount of generated $OH^\bullet$ radicals is determined by doubling the yield of I_3^- which corresponds to the amount of H_2O_2 measured using its absorbance at 350 nm (ε = 26,303 L mol^{-1} cm^{-1}). The reactions occurring during the KI sonication are:

$$OH\cdot + I^- \rightarrow OH^- + I\cdot \quad \text{Eq. (6)}$$

$$I\cdot + I^- \rightarrow I_2^{\cdot -} \quad \text{Eq. (7)}$$

$$2I_2^{\cdot -} \rightarrow I_2 + 2I^- \quad \text{Eq. (8)}$$

$$H_2O_2 + 2I^- + 2H^+ \rightarrow I_2 + 2H_2O \quad \text{Eq. (9)}$$

$$I_2 + I^- \rightarrow I_3^- \quad \text{Eq. (10)}$$

The generation of $OH^\bullet$ increased linearly with sonication time. However, the number of generated radicals was higher in the beaker under either continuous or intermittent pulse sonication compared to the Rosette cell (Figure 4-11). During the initial sonication using the beaker, the amount of $OH^\bullet$ increased and then started to decrease after 20 min, indicating that there is an optimum time for radical generation which may be due to a decrease in dissolved gases in the system. Since the solution volume was the same (15 mL) and the supplied power was constant (20 W), the increase in $OH^\bullet$ amount in the beaker compared to the Rosette cell is likely due to the difference in geometry. It may also be due to the liquid burst around the loops in the Rosette cell that might destroy some bubble nuclei and/or facilitate their migration to the surface of the liquid to finally evaporate. Interestingly, when the probe position was set at 1 cm from the bottom of the Rosette cell, the hydroxyl absorbance was 0.266. However, when the probe position was placed at 3.5 cm from the bottom of the Rosette cell, the absorbance value was 0.285. This shows the influence of the probe position in the Rosette cell on the $OH^\bullet$ generation. In the Rosette cell, intermittent sonication produced more radicals compared to continuous sonication (Figure 4-11), which is the reverse of sonicated samples in the beaker. Intermittent pulse sonication lowers the temperature in the reactor

during the off cycle, promoting the presence of dissolved gases necessary for the sonochemical activity.

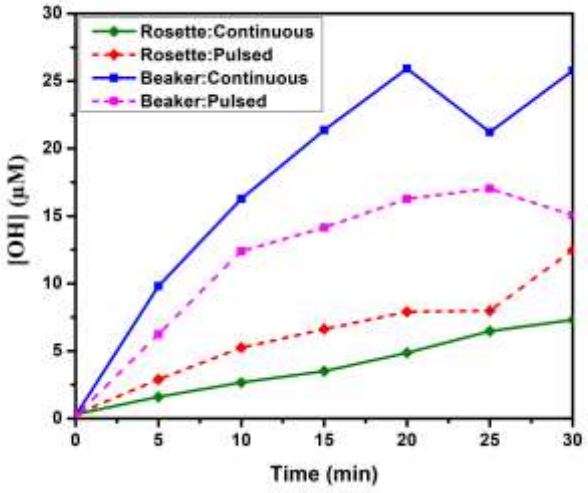

Figure 4-10 [OH•] yield in a Rosette cell and a beaker obtained from Weissler method at 20 kHz as a function of sonication time at fixed power of 20 W.

4.4.4.2 Physical effect of ultrasound on Au NP agglomeration

Under the seed-mediated protocol, Au NPs were produced before sonication or conventional stirring was applied (Figure 4-12A). Ultrasound irradiation efficiently minimized Au NP agglomerates through intense pressures generated from the cavitation process. Accordingly, Stucchi et al. and Boffito et al. reported that the sonication reduces particle size thereby increasing surface area and porosity [93]. When the seed-mediated protocol was performed under conventional stirring, the obtained Au NPs formed large agglomerates (Figure 4-12B). However, under ultrasound irradiation, the aggregated Au NPs were dispersed as submicronic aggregates (Figure 4-12C). In the two-step protocol, the action of ultrasonic irradiation at 100% amplitude (1.3 W mL^{-1}) led to the generation of Au NP agglomerates interconnected by a network of pores. Besides, the production of hydroxyl radicals increases with high ultrasonic power and in the presence of small particles. [75] Therefore, we infer that the reduction in pore size at 40 min

compared to 30 min sonication could be a result of further reduction of Au NPs on the surface by hydroxyl radicals generated during the extended synthesis time. In addition, high power can oxidize carbohydrates, such as glucose, as observed using FT-IR (Figure 4-6B). Sandrine et al. exploited the sonophysical and sonochemical effects of ultrasounds to provide medium homogeneity and chemical activation of glucose and sucrose [94]. In the absence of a catalyst, 96% of D-glucose were oxidized to glucuronic acid after 4 h using a 550 kHz ultrasound processor. The oxidation of glucose was confirmed with FT-IR by the presence of a carbonyl (C=O) band at 1723 cm−1 [95].

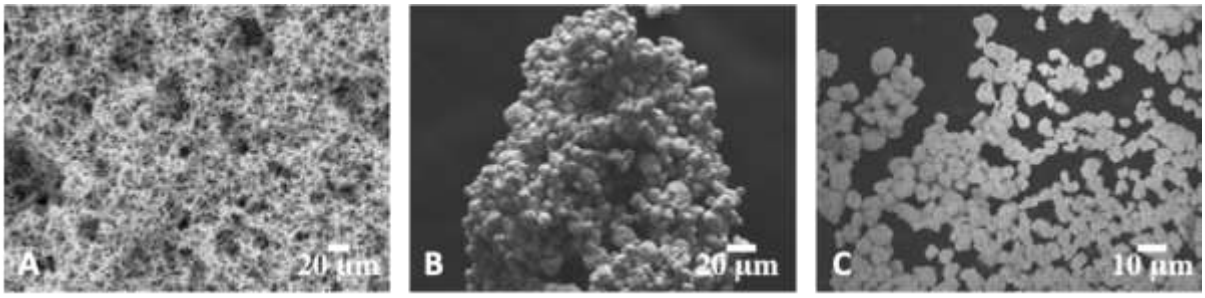

Figure 4-11 (A) Au NPs before the application of ultrasound or conventional stirring; (B) agglomerated Au NPs obtained by mechanical stirring; and (C) aggregated Au NPs after ultrasound irradiation.

4.5 Conclusion

Our results offer a novel perspective for the synthesis of Au NPs using ultrasound irradiation. The present study aimed to expand the synthesis of Au NPs by examining the effect of different parameters, such as the order of reagent addition, sonication mode and time, glucose concentration and pH, on the sonochemical formation of Au NPs using a 20 kHz ultrasound processor in a Rosette cell.The main outcomes of this work are: (1) high solvent volumes and low precursor concentrations are necessary to achieve the reduction of Au precursor when using ultrasound; (2) high concentrations of Au precursor in alkali environment result in the precipitation of large Au NPs; and (3) changes in pH of the reaction medium significantly affect the size and stability of obtained Au NPs. A high pH, especially above 9, corresponds to a significant redshift in the UV-Vis absorbance peak, indicating that large porous particles form from aggregated nanowires.

Moreover, the synthesis yield is affected by the different sonication approaches. Unambiguously, our results support that sonication throughout the mixing process rather than only after all solutions are combined has the strongest effect in terms of optical density and hence Au NP yield and stability. Furthermore, the formation of pores in the microstructure advocates for the use of low frequency ultrasounds in the synthesis of Au NPs as these make them suitable for the encapsulation/attachment of biomolecules of interest. Finally, our results offer an early perspective on analyzing the efficiency of different mixing methodologies in obtaining Au NPs of desired features and pave the way for the extensive comprehension of the physico-chemical phenomena occurring during the synthesis of valuable metallic nanomaterials via sonochemistry.

CHAPTER 5 GENERAL DISCUSSION

The synthesis of gold nanoparticles varies from the use of physical processes to break down bulk gold to the use of chemical or biological agents to form nanoparticles by nucleating atoms of gold in solution. Physical processes are limited either by the inability to control the shape while chemical and biological methods require the removal of material used to control the size and shape when applied for therapeutically. However, ultrasound can be used as a synthesis process without the addition of hazardous materials to effectively control the size and shape of Au NPs without further down-stream purification. Ultrasonication results in chemical and physical effects relating to the production of hydroxy radicals and other oxidizing species in association with shock waves that can nucleate and form Au NPs of controlled sizes and shapes.

Sonochemical technology offer novel synthesis routes, like radical and thermal reactions originating from high-temperature and high-strain cavitation bubbles. Various reducing species are produced in the course of the sonolysis of water and natural molecules. Metal ions are regularly reduced, and metallic nanoparticles may be fashioned in aqueous solutions using these reducing species. The types and/or quantities of the reducing species formed may be modified through various ultrasonic parameters like atmospheric gas, ultrasonic intensity, ultrasonic frequency, or arrangement of the oscillator. The reduction rate of metallic ions, and consequently the size and morphology of particles formed, is controlled by changing those parameters.

The aim of this work was to expand on the work of Zhang et al by using low frequency ultrasound (20 kHz) to synthesize anisotropic Au NPs. We studied the ultrasound assisted synthesis by modifying the concentration of the Au precursor, the reducing agent, the pH and ultrasound operational parameters of time, power and sonication mode. Likewise, we developed three synthesis methods using ultrasound to produce Au NP and Au MP with different anisotropic morphologies that were reproducible and can be directly applied for drug delivery without further purification steps. In a seed mediated method, we synthesized porous Au MPs by varying the sonication mode and time. In a two-step method, we synthesized porous Au NPs by increasing the solvent volume of two different ratios of Au stock solutions mixed with glucose and increasing the pH of the mixture. Finally, in a one-step method we compared the synthesis route with a conventional route to evaluate the effect of ultrasound on the synthesis process. We observed that

ultrasound effectively reduced the agglomerated Au NPs caused by pH changes in the medium compared to the conventional synthesis route. As a result, we showed that hydroxyl radicals obtained from the sonication process and pH changes to the reaction medium was essential in the production of Au NPs while the sonication mode and time was influential in the reduction and porosity of the obtained Au NPs. Furthermore, the formation of porous Au MP was accelerated by the action of ultrasound as contemporary sol-gel synthesis routes which would require prolonged aging to obtain microparticles.

CHAPTER 6 CONCLUSION AND RECOMMENDATIONS

The synthesis of gold nanoparticles in a Rosette cell was performed using a 20 kHz ultrasound processor. The addition of NaOH was necessary to obtain visual confirmation of gold nanoparticles as denoted by a color change and the appearance of a surface plasmon resonance at specific wavelengths above 520 nm. Furthermore, the pH of the final solution dictated the morphology of the formed gold particles. At pH 5, anisotropic gold microparticles of belt-like morphologies were produced, subsequently at pH 12 the gold nanoparticles were precipitated from the solution due to ultrasonic degradation of glucose and alkaline conditions. The operation of ultrasound at high solvent volumes and under continuous sonication was more effective at reducing the gold precursor compared to when the ultrasound was operated at low solvent volume and in intermittent mode. We observed that sonication time was important in obtaining porous gold nanoparticles, whereby 30 min of ultrasonication produced porous gold potatoes and 40 min of ultrasonication reduced the porosity of the Au microparticles. We compared our developed synthesis route with the chemical reduction method and observed that ultrasound effectively dispersed and reduced the size of porous gold microparticle agglomerates formed at pH 12 compared to the conventional chemical reduction route.

In the present project, we optimized the synthesis and operational parameters. However, the pH, sonication time and energy density are parameters that affect the morphology and optical properties of the produced gold nanoparticles. We recommend for future work a design of experiment to optimize these parameters, assessment of the yield and the functionalization of the obtained Au NP for nanomedicine application.

Moreover, we observed that the acoustic pressure in the Rosette cell was dependent on the sonication mode and the probe position. Therefore, to increase the number of radicals required for the synthesis it would be of interest to model the acoustic pressure at different probe positions and for different solvent volumes.

BIBLIOGRAPHY

[1] A. S. Thakor, J. Jokerst, C. Zavaleta, T. F. Massoud, and S. S. Gambhir, "Gold nanoparticles: A revival in precious metal administration to patients," *Nano Letters*, vol. 11, no. 10. NIH Public Access, pp. 4029–4036, Oct. 12, 2011, doi: 10.1021/nl202559p.

[2] J. Guo, K. Rahme, Y. He, L. L. Li, J. D. Holmes, and C. M. O'Driscoll, "Gold nanoparticles enlighten the future of cancer theranostics," *International Journal of Nanomedicine*, vol. 12. Dove Medical Press Ltd., pp. 6131–6152, Aug. 22, 2017, doi: 10.2147/IJN.S140772.

[3] D. R. Brenner *et al.*, "Projected estimates of cancer in Canada in 2020," *CMAJ*, vol. 192, no. 9, pp. E199–E205, Mar. 2020, doi: 10.1503/cmaj.191292.

[4] J. Zugazagoitia, C. Guedes, S. Ponce, I. Ferrer, S. Molina-Pinelo, and L. Paz-Ares, "Current Challenges in Cancer Treatment," *Clinical Therapeutics*, vol. 38, no. 7. Excerpta Medica Inc., pp. 1551–1566, Jul. 01, 2016, doi: 10.1016/j.clinthera.2016.03.026.

[5] W. H. De Jong and P. J. A. Borm, "Drug delivery and nanoparticles: Applications and hazards," *International Journal of Nanomedicine*, vol. 3, no. 2. Dove Press, pp. 133–149, 2008, doi: 10.2147/ijn.s596.

[6] X. Bai *et al.*, "The Basic Properties of Gold Nanoparticles and their Applications in Tumor Diagnosis and Treatment," *Int. J. Mol. Sci.*, vol. 21, no. 7, p. 2480, Apr. 2020, doi: 10.3390/ijms21072480.

[7] "Gold - Properties, occurrences, and uses | Britannica." https://www.britannica.com/science/gold-chemical-element/Properties-occurrences-and-uses (accessed Mar. 18, 2021).

[8] K. Sun, M. Kohyama, S. Tanaka, and S. Takeda, "Understanding of the activity difference between nanogold and bulk gold by relativistic effects," *J. Energy Chem.*, 2015, doi: 10.1016/j.jechem.2015.06.006.

[9] V. Petkov, Y. Peng, G. Williams, B. Huang, D. Tomalia, and Y. Ren, "Structure of gold nanoparticles suspended in water studied by x-ray diffraction and computer simulations," *Phys. Rev. B - Condens. Matter Mater. Phys.*, 2005, doi: 10.1103/PhysRevB.72.195402.

[10] K. Hussain and T. Hussain, "Gold Nanoparticles:A Boon to Drug Delivery System," *South*

Indian J. Biol. Sci., vol. 1, no. 3, p. 128, 2015, doi: 10.22205/sijbs/2015/v1/i3/100407.

[11] P. Pedrosa, R. Vinhas, A. Fernandes, and P. V. Baptista, "Gold nanotheranostics: Proof-of-concept or clinical tool?," *Nanomaterials*, vol. 5, no. 4. MDPI AG, pp. 1853–1879, Nov. 03, 2015, doi: 10.3390/nano5041853.

[12] E. C. Dreaden, A. M. Alkilany, X. Huang, C. J. Murphy, and M. A. El-Sayed, "The golden age: Gold nanoparticles for biomedicine," *Chemical Society Reviews*, vol. 41, no. 7. pp. 2740–2779, 2012, doi: 10.1039/c1cs15237h.

[13] I. Blakey, Z. Merican, and K. J. Thurecht, "A method for controlling the aggregation of gold nanoparticles: Tuning of optical and spectroscopic properties," *Langmuir*, 2013, doi: 10.1021/la401361u.

[14] J. B. Vines, J. H. Yoon, N. E. Ryu, D. J. Lim, and H. Park, "Gold nanoparticles for photothermal cancer therapy," *Frontiers in Chemistry*. 2019, doi: 10.3389/fchem.2019.00167.

[15] M. Sengani, A. M. Grumezescu, and V. D. Rajeswari, "Recent trends and methodologies in gold nanoparticle synthesis – A prospective review on drug delivery aspect," *OpenNano*, vol. 2. Elsevier Inc, pp. 37–46, 2017, doi: 10.1016/j.onano.2017.07.001.

[16] L. F. De Freitas, G. H. C. Varca, J. G. D. S. Batista, and A. B. Lugão, "An overview of the synthesis of gold nanoparticles using radiation technologies," *Nanomaterials*, vol. 8, no. 11. MDPI AG, p. 939, Nov. 15, 2018, doi: 10.3390/nano8110939.

[17] V. Piotto, L. Litti, and M. Meneghetti, "Synthesis and Shape Manipulation of Anisotropic Gold Nanoparticles by Laser Ablation in Solution," *J. Phys. Chem. C*, vol. 124, no. 8, pp. 4820–4826, Feb. 2020, doi: 10.1021/acs.jpcc.9b10793.

[18] "Synthesis of gold nanoparticles - Chemistry LibreTexts." https://chem.libretexts.org/Bookshelves/Analytical_Chemistry/Supplemental_Modules_(Analytical_Chemistry)/Analytical_Sciences_Digital_Library/Active_Learning/Contextual_Modules/Optical_Properties_of_Gold_Nanoparticles/04_Instructor's_Guide/02_Synthesis_of_gold_nanoparticles (accessed Apr. 09, 2021).

[19] C. Daruich De Souza, B. Ribeiro Nogueira, and M. E. C. M. Rostelato, "Review of the methodologies used in the synthesis gold nanoparticles by chemical reduction," *Journal of*

Alloys and Compounds, vol. 798. Elsevier Ltd, pp. 714–740, Aug. 25, 2019, doi: 10.1016/j.jallcom.2019.05.153.

[20] C. Daruich De Souza, B. Ribeiro Nogueira, and M. E. C. M. Rostelato, "Review of the methodologies used in the synthesis gold nanoparticles by chemical reduction," *Journal of Alloys and Compounds*, vol. 798. Elsevier B.V, pp. 714–740, 2019, doi: 10.1016/j.jallcom.2019.05.153.

[21] J. A. Gutierrez, J. J. Silber, R. D. Falcone, and N. M. Correa, "Modified reverse micelle method as facile way to obtain several gold nanoparticle morphologies," *J. Mol. Liq.*, vol. 331, p. 115709, 2021, doi: 10.1016/j.molliq.2021.115709.

[22] A. M. Vostrikova *et al.*, "One step hydrothermal functionalization of gold nanoparticles with folic acid," *Colloids Surfaces B Biointerfaces*, 2019, doi: 10.1016/j.colsurfb.2019.05.072.

[23] K. A. Kamath, I. Nasim, and S. Rajesh, "Biogenic Synthesis of Gold Nanoparticles from Aspartic Acid - A Preliminary Study," *J. Pharm. Res. Int.*, pp. 21–27, Aug. 2020, doi: 10.9734/jpri/2020/v32i1830685.

[24] Y. P. Jia *et al.*, "Effects of Cetyltrimethylammonium Bromide on the Toxicity of Gold Nanorods Both In Vitro and In Vivo: Molecular Origin of Cytotoxicity and Inflammation," *Small Methods*, 2020, doi: 10.1002/smtd.201900799.

[25] J. E. Ortiz-Castillo, R. C. Gallo-Villanueva, M. J. Madou, and V. H. Perez-Gonzalez, "Anisotropic gold nanoparticles: A survey of recent synthetic methodologies," *Coordination Chemistry Reviews*, vol. 425. Elsevier B.V., p. 213489, Dec. 15, 2020, doi: 10.1016/j.ccr.2020.213489.

[26] N. Li, P. Zhao, and D. Astruc, "Anisotropic gold nanoparticles: Synthesis, properties, applications, and toxicity," *Angew. Chemie - Int. Ed.*, vol. 53, no. 7, pp. 1756–1789, 2014, doi: 10.1002/anie.201300441.

[27] Y. Ohara *et al.*, "Seed-mediated gold nanoparticle synthesis via photochemical reaction of benzoquinone," *Colloids Surfaces A Physicochem. Eng. Asp.*, vol. 586, p. 124209, Feb. 2020, doi: 10.1016/j.colsurfa.2019.124209.

[28] Z. Liao *et al.*, "Dopamine-assisted one-pot synthesis of gold nanoworms and their application as photothermal agents," *J. Colloid Interface Sci.*, vol. 562, pp. 81–90, Mar.

2020, doi: 10.1016/j.jcis.2019.11.055.

[29] V. Oestreicher, C. Huck-Iriart, G. Soler-Illia, P. C. Angelomé, and M. Jobbágy, “Mild Homogeneous Synthesis of Gold Nanoparticles through the Epoxide Route: Kinetics, Mechanisms, and Related One-Pot Composites,” *Chem. - A Eur. J.*, vol. 26, no. 14, pp. 3157–3165, Mar. 2020, doi: 10.1002/chem.201905335.

[30] S. J. Amina and B. Guo, “A review on the synthesis and functionalization of gold nanoparticles as a drug delivery vehicle,” *International Journal of Nanomedicine*, vol. 15. Dove Medical Press Ltd, pp. 9823–9857, Dec. 07, 2020, doi: 10.2147/IJN.S279094.

[31] K. Kalimuthu, B. S. Cha, S. Kim, and K. S. Park, “Eco-friendly synthesis and biomedical applications of gold nanoparticles: A review,” *Microchemical Journal*, vol. 152. Elsevier Inc., p. 104296, Jan. 01, 2020, doi: 10.1016/j.microc.2019.104296.

[32] K. X. Lee *et al.*, “Recent developments in the facile bio-synthesis of gold nanoparticles (AuNPs) and their biomedical applications,” *International Journal of Nanomedicine*, vol. 15. Dove Medical Press Ltd., pp. 275–300, 2020, doi: 10.2147/IJN.S233789.

[33] S. R. Bhuvanasree, D. Harini, A. Rajaram, and R. Rajaram, “Rapid synthesis of gold nanoparticles with Cissus quadrangularis extract using microwave irradiation,” *Spectrochim. Acta - Part A Mol. Biomol. Spectrosc.*, vol. 106, pp. 190–196, Apr. 2013, doi: 10.1016/j.saa.2012.12.076.

[34] J. A. Fuentes-García, J. Santoyo-Salzar, E. Rangel-Cortes, G. F. Goya, V. Cardozo-Mata, and J. A. Pescador-Rojas, “Effect of ultrasonic irradiation power on sonochemical synthesis of gold nanoparticles,” *Ultrason. Sonochem.*, vol. 70, p. 105274, 2021, doi: 10.1016/j.ultsonch.2020.105274.

[35] A. Shanei and M. M. Shanei, “Effect of gold nanoparticle size on acoustic cavitation using chemical dosimetry method,” *Ultrason. Sonochem.*, vol. 34, pp. 45–50, 2017, doi: 10.1016/j.ultsonch.2016.05.010.

[36] A. Aqil, H. Serwas, J. L. Delplancke, R. Jérôme, C. Jérôme, and L. Canet, “Ultrasonics Sonochemistry Preparation of stable suspensions of gold nanoparticles in water by sonoelectrochemistry,” vol. 15, pp. 1055–1061, 2008, doi: 10.1016/j.ultsonch.2008.04.004.

[37] L. M. Cubillana-Aguilera, M. Franco-Romano, M. L. A. Gil, I. Naranjo-Rodríguez, J. L.

Hidalgo-Hidalgo De Cisneros, and J. M. Palacios-Santander, “New, fast and green procedure for the synthesis of gold nanoparticles based on sonocatalysis,” *Ultrason. Sonochem.*, vol. 18, no. 3, pp. 789–794, 2011, doi: 10.1016/j.ultsonch.2010.10.009.

[38] T. Sakai, H. Enomoto, H. Sakai, and M. Abe, “Hydrogen-assisted fabrication of spherical gold nanoparticles through sonochemical reduction of tetrachloride gold(III) ions in water,” *Ultrason. Sonochem.*, vol. 21, no. 3, pp. 946–950, 2014, doi: 10.1016/j.ultsonch.2013.12.010.

[39] K. Okitsu and S. Semboshi, “Synthesis of Au nanorods via autocatalytic growth of Au seeds formed by sonochemical reduction of Au(I): Relation between formation rate and characteristic of Au nanorods,” *Ultrason. Sonochem.*, vol. 69, no. May, p. 105229, 2020, doi: 10.1016/j.ultsonch.2020.105229.

[40] K. Okitsu, I. Kurisaka, B. Nanzai, N. Takenaka, and H. Bandow, “Mechanism for sonochemical reduction of Au(III) in aqueous butanol solution under Ar based on the analysis of gaseous and water-soluble products,” *Ultrason. Sonochem.*, vol. 69, p. 105241, Dec. 2020, doi: 10.1016/j.ultsonch.2020.105241.

[41] M. Y. Wei, L. Famouri, L. Carroll, Y. Lee, and P. Famouri, “Rapid and efficient sonochemical formation of gold nanoparticles under ambient conditions using functional alkoxysilane,” *Ultrason. Sonochem.*, vol. 20, no. 1, pp. 610–617, 2013, doi: 10.1016/j.ultsonch.2012.07.028.

[42] J. E. Park, M. Atobe, and T. Fuchigami, “Synthesis of multiple shapes of gold nanoparticles with controlled sizes in aqueous solution using ultrasound,” *Ultrason. Sonochem.*, vol. 13, no. 3, pp. 237–241, Apr. 2006, doi: 10.1016/j.ultsonch.2005.04.003.

[43] Q. Shen, Q. Min, J. Shi, L. Jiang, W. Hou, and J. J. Zhu, “Synthesis of stabilizer-free gold nanoparticles by pulse sonoelectrochemical method,” *Ultrason. Sonochem.*, vol. 18, no. 1, pp. 231–237, Jan. 2011, doi: 10.1016/j.ultsonch.2010.05.011.

[44] P. T. Huynh, G. D. Nguyen, K. Thi Le Tran, T. Minh Ho, V. Q. Lam, and T. V. K. Ngo, “Rapid and green preparation of multi-branched gold nanoparticles using surfactant-free, combined ultrasound-assisted method,” *Processes*, vol. 9, no. 1, pp. 1–16, 2021, doi: 10.3390/pr9010112.

[45] V. Amendola and M. Meneghetti, “Size Evaluation of Gold Nanoparticles by UV−vis Spectroscopy,” *J. Phys. Chem. C*, vol. 113, no. 11, pp. 4277–4285, Feb. 2009, doi: 10.1021/jp8082425.

[46] W. Haiss, N. T. K. Thanh, J. Aveyard, and D. G. Fernig, “Determination of size and concentration of gold nanoparticles from UV-Vis spectra,” *Anal. Chem.*, vol. 79, no. 11, pp. 4215–4221, Apr. 2007, doi: 10.1021/ac0702084.

[47] F. S. Rocha, A. J. Gomes, C. N. Lunardi, S. Kaliaguine, and G. S. Patience, “Experimental methods in chemical engineering: Ultraviolet visible spectroscopy-UV-Vis,” *Can. J. Chem. Eng.*, vol. 96, no. 12, pp. 2512–2517, Dec. 2018, doi: 10.1002/cjce.23344.

[48] M. O. Guerrero-Pérez and G. S. Patience, “Experimental methods in chemical engineering: Fourier transform infrared spectroscopy—FTIR,” *Can. J. Chem. Eng.*, vol. 98, no. 1, pp. 25–33, Jan. 2020, doi: 10.1002/cjce.23664.

[49] K. Sztandera, M. Gorzkiewicz, and B. Klajnert-Maculewicz, “Gold Nanoparticles in Cancer Treatment,” *Molecular Pharmaceutics*, vol. 16, no. 1. pp. 1–23, 2019, doi: 10.1021/acs.molpharmaceut.8b00810.

[50] U. Chude-Okonkwo, R. Malekian, and B. T. Maharaj, “Nanosystems and Devices for Advanced Targeted Nanomedical Applications,” Springer, Cham, 2019, pp. 39–58.

[51] S. Hossen, M. K. Hossain, M. K. Basher, M. N. H. Mia, M. T. Rahman, and M. J. Uddin, “Smart nanocarrier-based drug delivery systems for cancer therapy and toxicity studies: A review,” *Journal of Advanced Research*, vol. 15. Elsevier B.V., pp. 1–18, Jan. 01, 2019, doi: 10.1016/j.jare.2018.06.005.

[52] X. Hu, Y. Zhang, T. Ding, J. Liu, and H. Zhao, “Multifunctional Gold Nanoparticles: A Novel Nanomaterial for Various Medical Applications and Biological Activities,” *Frontiers in Bioengineering and Biotechnology*, vol. 8. Frontiers Media S.A., p. 990, Aug. 13, 2020, doi: 10.3389/fbioe.2020.00990.

[53] S. A. Bansal, V. Kumar, J. Karimi, A. P. Singh, and S. Kumar, “Role of gold nanoparticles in advanced biomedical applications,” 2020, doi: 10.1039/d0na00472c.

[54] I. Khan, K. Saeed, and I. Khan, “Nanoparticles: Properties, applications and toxicities,” *Arab. J. Chem.*, vol. 12, no. 7, pp. 908–931, 2019, doi: 10.1016/j.arabjc.2017.05.011.

[55] Y. Tian, S. Shen, J. Feng, X. Jiang, and W. Yang, “Mussel-Inspired Gold Hollow Superparticles for Photothermal Therapy,” *Adv. Healthc. Mater.*, vol. 4, no. 7, pp. 1009–1014, May 2015, doi: 10.1002/adhm.201400787.

[56] S. Bale, A. Khurana, A. S. S. Reddy, M. Singh, and C. Godugu, “Overview on therapeutic applications of microparticulate drug delivery systems,” *Crit. Rev. Ther. Drug Carrier Syst.*, vol. 33, no. 4, pp. 309–361, 2016, doi: 10.1615/CritRevTherDrugCarrierSyst.2016015798.

[57] R. Arvizo, R. Bhattacharya, and P. Mukherjee, “Gold nanoparticles: Opportunities and challenges in nanomedicine,” *Expert Opin. Drug Deliv.*, vol. 7, no. 6, pp. 753–763, 2010, doi: 10.1517/17425241003777010.

[58] X. Huang and M. A. El-Sayed, “Gold nanoparticles: Optical properties and implementations in cancer diagnosis and photothermal therapy,” *Journal of Advanced Research*, vol. 1, no. 1. Elsevier, pp. 13–28, Jan. 01, 2010, doi: 10.1016/j.jare.2010.02.002.

[59] B. Nikoobakht and M. A. El-Sayed, “Preparation and growth mechanism of gold nanorods (NRs) using seed-mediated growth method,” *Chem. Mater.*, vol. 15, no. 10, pp. 1957–1962, Apr. 2003, doi: 10.1021/cm020732l.

[60] X. Huang, I. H. El-Sayed, W. Qian, and M. A. El-Sayed, “Cancer cell imaging and photothermal therapy in the near-infrared region by using gold nanorods,” *J. Am. Chem. Soc.*, vol. 128, no. 6, pp. 2115–2120, Jan. 2006, doi: 10.1021/ja057254a.

[61] Y. Wang *et al.*, “Comparison Study of Gold Nanohexapods, Nanorods, and Nanocages for Photothermal Cancer Treatment,” *ACS Nano*, vol. 7, no. 3, pp. 2068–2077, Feb. 2013, doi: 10.1021/nn304332s.

[62] N. Li, P. Zhao, and D. Astruc, “Anisotropic Gold Nanoparticles: Synthesis, Properties, Applications, and Toxicity,” *Angew. Chemie Int. Ed.*, vol. 53, no. 7, pp. 1756–1789, Feb. 2014, doi: 10.1002/anie.201300441.

[63] R. Ravanshad *et al.*, “Application of nanoparticles in cancer detection by Raman scattering based techniques,” *Nano Rev. Exp.*, vol. 9, no. 1, p. 1373551, Jan. 2018, doi: 10.1080/20022727.2017.1373551.

[64] S. Kalmodia *et al.*, “Synthesis and characterization of surface-enhanced Raman-scattered gold nanoparticles,” *Int. J. Nanomedicine*, vol. 8, pp. 4327–4338, Nov. 2013, doi:

10.2147/IJN.S49447.

[65] S. Eustis and M. El-Sayed, “Aspect Ratio Dependence of the Enhanced Fluorescence Intensity of Gold Nanorods: Experimental and Simulation Study,” *J. Phys. Chem. B*, vol. 109, no. 34, pp. 16350–16356, Aug. 2005, doi: 10.1021/jp052951a.

[66] M. Sharifi *et al.*, “Plasmonic and chiroplasmonic nanobiosensors based on gold nanoparticles,” *Talanta*, vol. 212, p. 120782, May 2020, doi: 10.1016/j.talanta.2020.120782.

[67] S. Suvarna *et al.*, “Synthesis of a novel glucose capped gold nanoparticle as a better theranostic candidate,” *PLoS One*, vol. 12, no. 6, pp. 1–15, 2017, doi: 10.1371/journal.pone.0178202.

[68] S. Chairam, W. Konkamdee, and R. Parakhun, “Starch-supported gold nanoparticles and their use in 4-nitrophenol reduction Starch-supported gold nanoparticles in 4-nitrophenol reduction,” *J. Saudi Chem. Soc.*, vol. 21, no. 6, pp. 656–663, 2017, doi: 10.1016/j.jscs.2015.11.001.

[69] V. Springer, M. A. Segundo, M. E. Centurión, and M. Avena, “Fully-programmable synthesis of sucrose-mediated gold nanoparticles for detection of ciprofloxacin,” *Mater. Chem. Phys.*, vol. 238, p. 121917, Dec. 2019, doi: 10.1016/j.matchemphys.2019.121917.

[70] J. K. Patra *et al.*, “Nano based drug delivery systems : recent developments and future prospects,” *J. Nanobiotechnology*, pp. 1–33, 2018, doi: 10.1186/s12951-018-0392-8.

[71] M. Hujjatul Islam, M. T. Y. Paul, O. S. Burheim, and B. G. Pollet, “Recent developments in the sonoelectrochemical synthesis of nanomaterials,” *Ultrason. Sonochem.*, vol. 59, no. July, p. 104711, 2019, doi: 10.1016/j.ultsonch.2019.104711.

[72] K. Pacławski, D. A. Zając, M. Borowiec, C. Kapusta, and K. Fitzner, “EXAFS studies on the reaction of gold (III) chloride complex ions with sodium hydroxide and glucose,” *J. Phys. Chem. A*, vol. 114, no. 44, pp. 11943–11947, 2010, doi: 10.1021/jp102836f.

[73] G. Chatel, “How sonochemistry contributes to green chemistry?,” *Ultrason. Sonochem.*, 2018, doi: 10.1016/j.ultsonch.2017.03.029.

[74] T. Leong, M. Ashokkumar, and K. Sandra, “The fundamentals of power ultrasound - A review,” 2011.

[75] H. Laajimi, M. Mattia, R. S. Stein, C. L. Bianchi, and D. C. Boffito, “Electron paramagnetic resonance of sonicated powder suspensions in organic solvents,” *Ultrason. Sonochem.*, p. 105544, Mar. 2021, doi: 10.1016/j.ultsonch.2021.105544.

[76] Z. Khani, D. Schieppati, C. L. Bianchi, and D. C. Boffito, “The sonophotocatalytic degradation of pharmaceuticals in water by Mnox-Tio2 systems with tuned band-gaps,” *Catalysts*, vol. 9, no. 11, pp. 1–21, 2019, doi: 10.3390/catal9110949.

[77] H. Xu, B. W. Zeiger, and K. S. Suslick, “Sonochemical synthesis of nanomaterials,” *Chemical Society Reviews*, vol. 42, no. 7. The Royal Society of Chemistry, pp. 2555–2567, Mar. 11, 2013, doi: 10.1039/c2cs35282f.

[78] K. Yasui, “Fundamentals of acoustic cavitation and sonochemistry,” in *Theoretical and Experimental Sonochemistry Involving Inorganic Systems*, Dordrecht: Springer Netherlands, 2011, pp. 1–29.

[79] S. Kentish and M. Ashokkumar, “The physical and chemical effects of ultrasound,” in *Food Engineering Series*, Springer, 2011, pp. 1–12.

[80] M. Ashokkumar, “The characterization of acoustic cavitation bubbles - An overview,” in *Ultrasonics Sonochemistry*, Jul. 2011, vol. 18, no. 4, pp. 864–872, doi: 10.1016/j.ultsonch.2010.11.016.

[81] R. J. Wood, J. Lee, and M. J. Bussemaker, “A parametric review of sonochemistry: Control and augmentation of sonochemical activity in aqueous solutions,” *Ultrasonics Sonochemistry*, vol. 38. Elsevier B.V., pp. 351–370, Sep. 01, 2017, doi: 10.1016/j.ultsonch.2017.03.030.

[82] J. S. Taurozzi, V. A. Hackley, and M. R. Wiesner, “Ultrasonic dispersion of nanoparticles for environmental, health and safety assessment issues and recommendations,” *Nanotoxicology*, vol. 5, no. 4, pp. 711–729, 2011, doi: 10.3109/17435390.2010.528846.

[83] M. Ashokkumar *et al.*, *Handbook of ultrasonics and sonochemistry*. 2016.

[84] J. J. Hinman and K. S. Suslick, “Nanostructured Materials Synthesis Using Ultrasound,” *Top. Curr. Chem.*, vol. 375, no. 1, pp. 1–36, 2017, doi: 10.1007/s41061-016-0100-9.

[85] M. Stucchi, A. Elfiad, M. Rigamonti, H. Khan, and D. C. Boffito, “Water treatment: Mn-

TiO2 synthesized by ultrasound with increased aromatics adsorption," *Ultrason. Sonochem.*, vol. 44, pp. 272–279, Jun. 2018, doi: 10.1016/j.ultsonch.2018.01.023.

[86] F. Ali *et al.*, "Effect of sonication conditions: Solvent, time, temperature and reactor type on the preparation of micron sized vermiculite particles," *Ultrason. Sonochem.*, vol. 21, no. 3, pp. 1002–1009, May 2014, doi: 10.1016/j.ultsonch.2013.10.010.

[87] D. C. Boffito, S. Mansi, J.-M. Leveque, C. Pirola, C. L. Bianchi, and G. S. Patience, "Ultrafast Biodiesel Production Using Ultrasound in Batch and Continuous Reactors," *ACS Sustain. Chem. & Eng.*, vol. 1, no. 11, pp. 1432–1439, Sep. 2013, doi: 10.1021/sc400161s.

[88] R. F. Contamine, A. M. Wilhelm, J. Berlan, and H. Delmas, "Power measurement in sonochemistry," *Ultrason. - Sonochemistry*, vol. 2, no. 1, pp. S43–S47, Jan. 1995, doi: 10.1016/1350-4177(94)00010-P.

[89] T. Thanh Nguyen, Y. Asakura, S. Koda, and K. Yasuda, "Dependence of cavitation, chemical effect, and mechanical effect thresholds on ultrasonic frequency," *Ultrason. Sonochem.*, vol. 39, pp. 301–306, Nov. 2017, doi: 10.1016/j.ultsonch.2017.04.037.

[90] J. Zhang, J. Du, B. Han, Z. Liu, T. Jiang, and Z. Zhang, "Sonochemical formation of single-crystalline gold nanobelts," *Angew. Chemie - Int. Ed.*, vol. 45, no. 7, pp. 1116–1119, 2006, doi: 10.1002/anie.200503762.

[91] L. M. Cubillana-Aguilera, M. Franco-Romano, M. L. A. Gil, I. Naranjo-Rodríguez, J. L. Hidalgo-Hidalgo De Cisneros, and J. M. Palacios-Santander, "New, fast and green procedure for the synthesis of gold nanoparticles based on sonocatalysis," *Ultrason. Sonochem.*, vol. 18, no. 3, pp. 789–794, May 2011, doi: 10.1016/j.ultsonch.2010.10.009.

[92] A. D. Daigle and J. J. Belbruno, "Density functional theory study of the adsorption of nitrogen and sulfur atoms on gold (111), (100), and (211) surfaces," *J. Phys. Chem. C*, vol. 115, no. 46, pp. 22987–22997, Nov. 2011, doi: 10.1021/jp2071327.

[93] D. C. Boffito *et al.*, "Ultrasonic enhancement of the acidity, surface area and free fatty acids esterification catalytic activity of sulphated ZrO2-TiO2 systems," *J. Catal.*, vol. 297, pp. 17–26, Jan. 2013, doi: 10.1016/j.jcat.2012.09.013.

[94] S. Brochette-Lemoine, S. Trombotto, D. Joannard, G. Descotes, A. Bouchu, and Y.

Queneau, “Ultrasound in carbohydrate chemistry: Sonophysical glucose oligomerisation and sonocatalysed sucrose oxidation,” *Ultrason. Sonochem.*, vol. 7, no. 4, pp. 157–161, Oct. 2000, doi: 10.1016/S1350-4177(99)00035-8.

[95] P. N. Amaniampong *et al.*, “Selective and Catalyst-free Oxidation of D-Glucose to D-Glucuronic acid induced by High-Frequency Ultrasound,” *Sci. Rep.*, vol. 7, no. 1, pp. 1–8, Jan. 2017, doi: 10.1038/srep40650.

APPENDIX A SUPPLEMENTAL INFORMATION

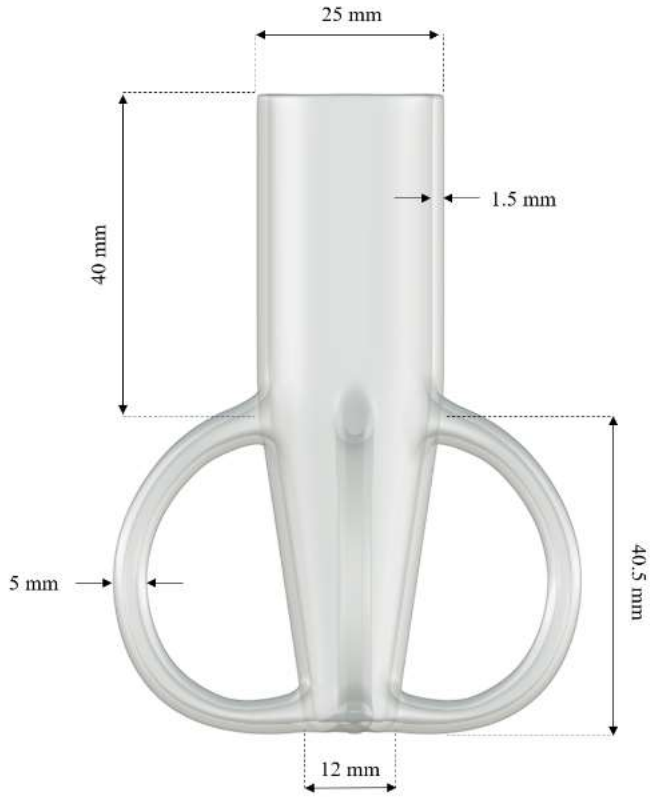

Figure S1. *Rosette cell reactor adopted for the synthesis of Au NPs.*

Effect of $C_6H_{12}O_6$ concentrations

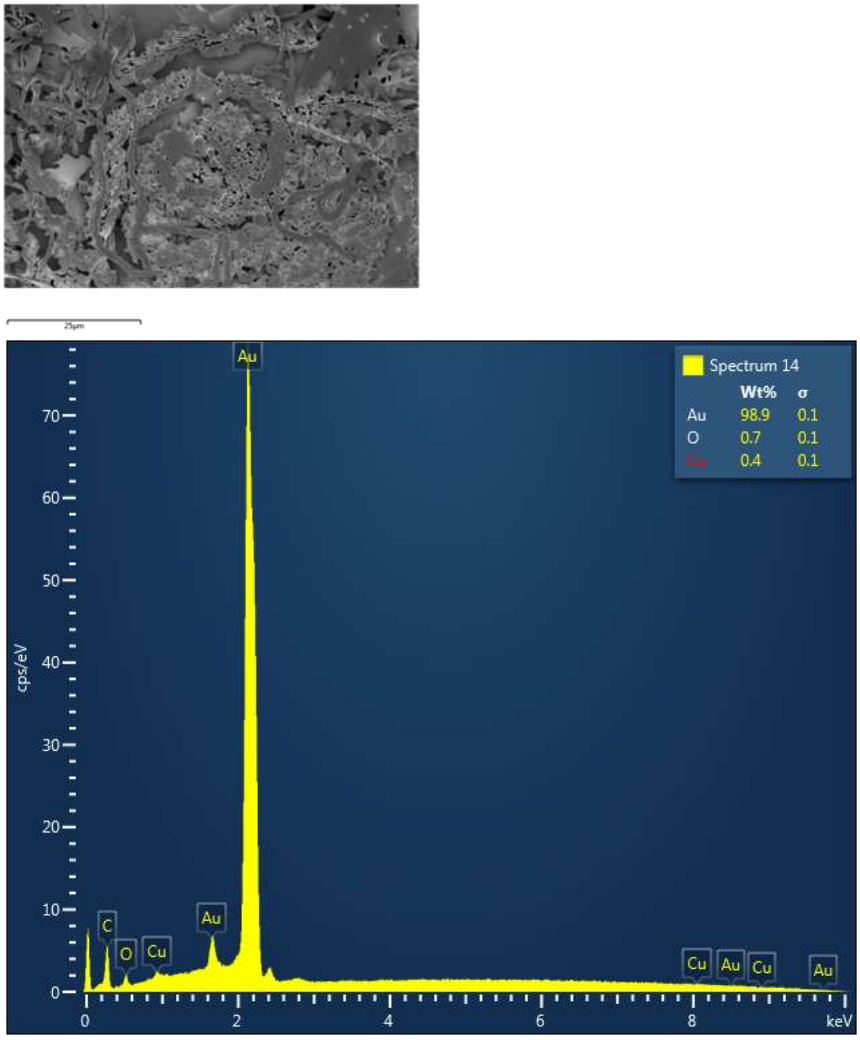

Figure S2: SEM and EDS of Au NPs synthesized at pH 7 (10 mM $C_6H_{12}O_6$).

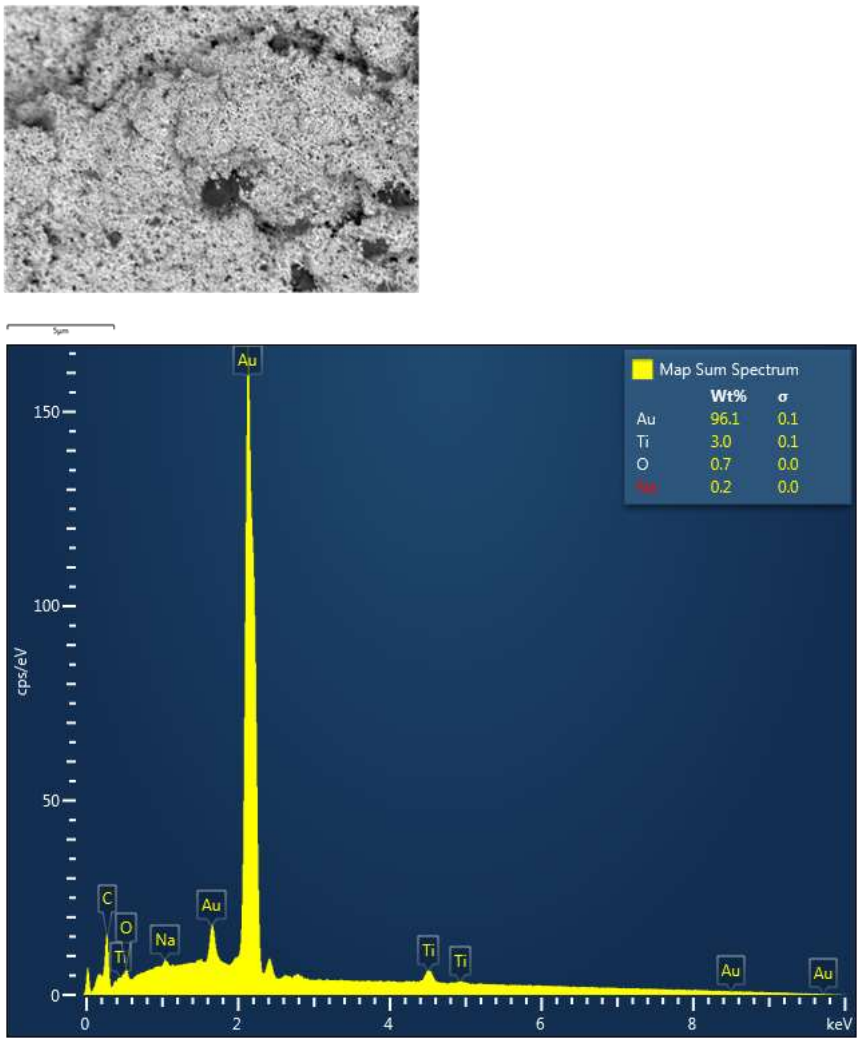

Figure S3: SEM and EDS of Au NPs synthesized at pH 7 (20 mM $C_6H_{12}O_6$)

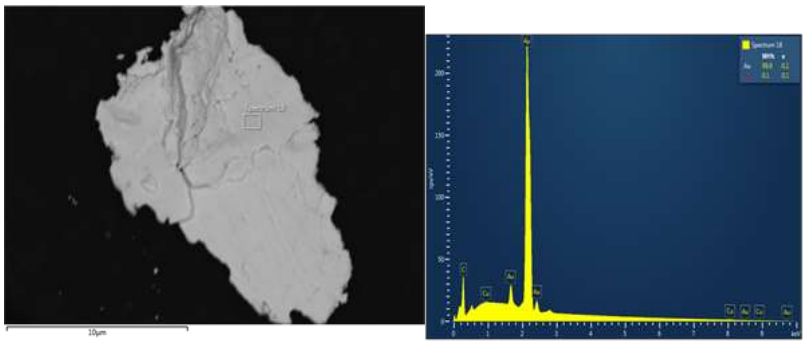

Figure S4: SEM and EDS of Au NPs synthesized at pH 7 (40 mM $C_6H_{12}O_6$).

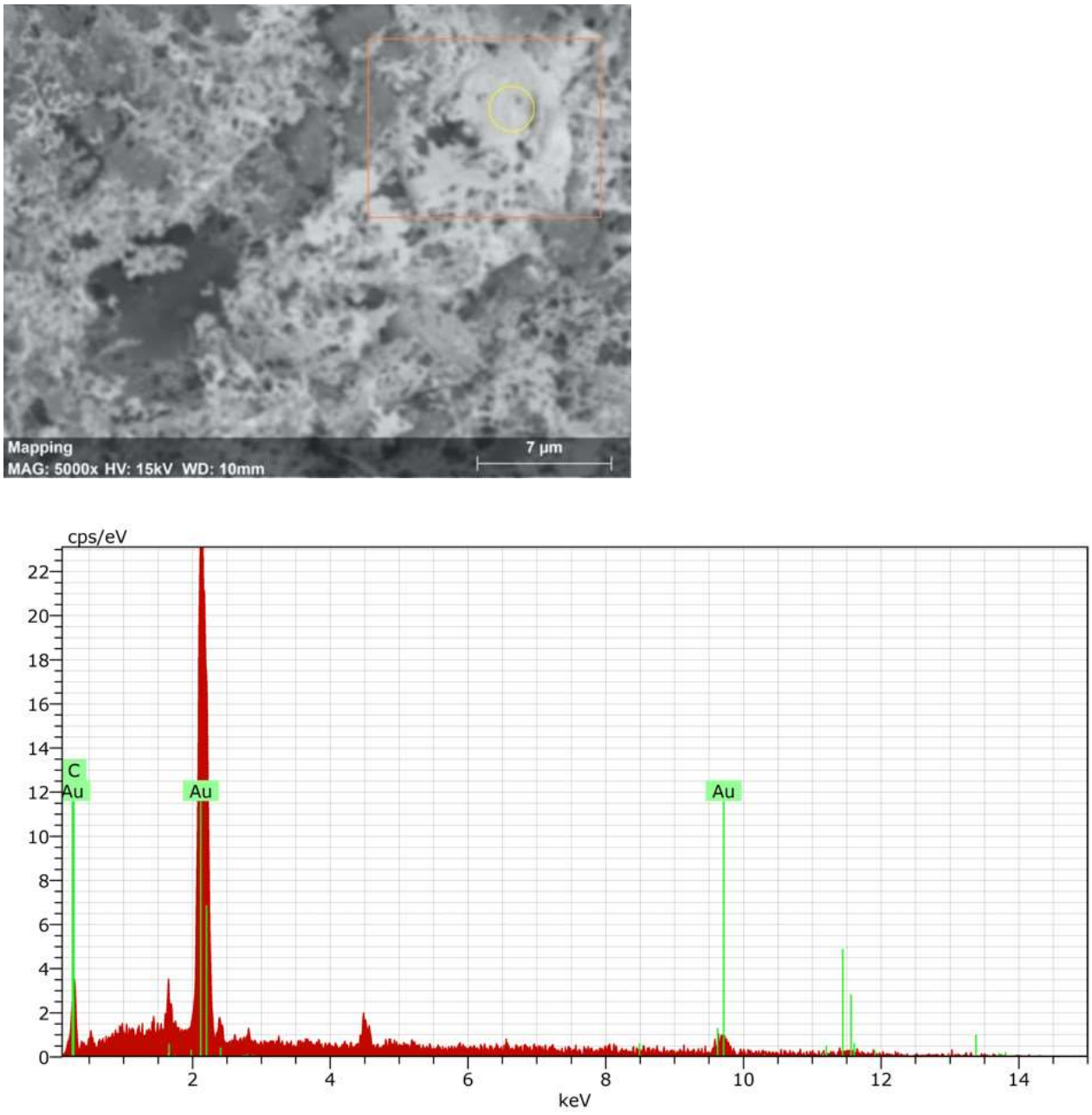

Figure S5. *EDS Mapping of Au MPs produced at pH 5.*

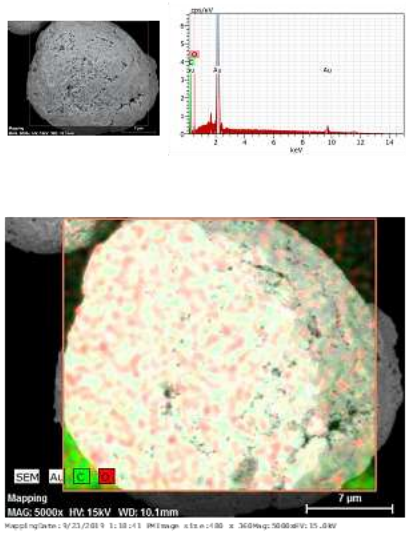

Figure S6. *EDS Mapping of Au MPs produced at pH 12.*

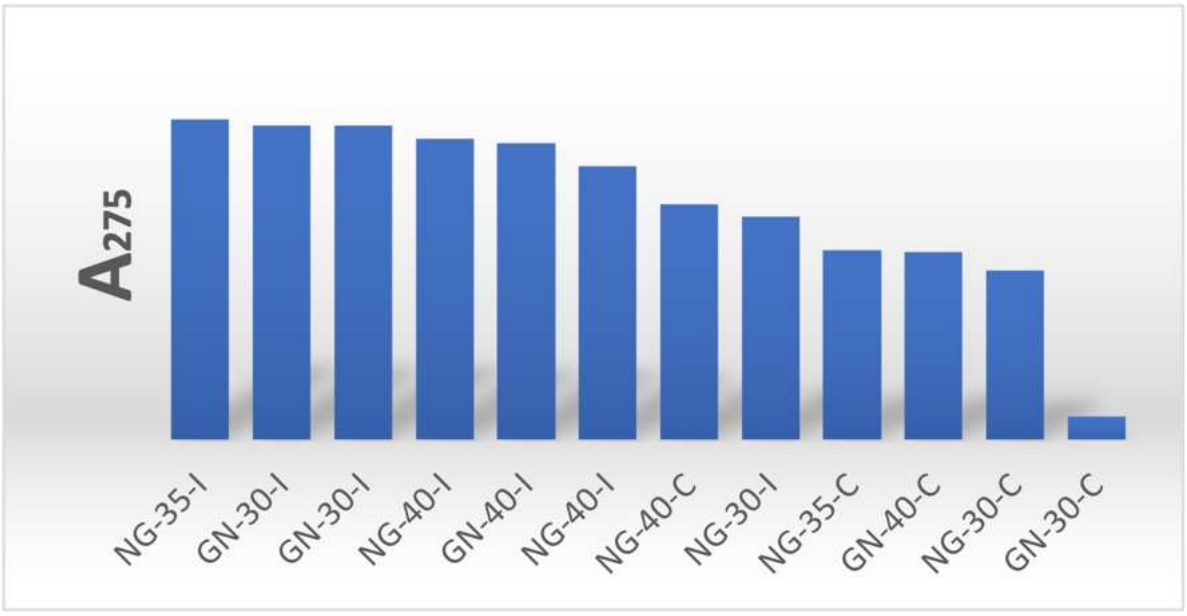

Figure S7. Influence of sonication mode (I: Intermittent and C: Continuous) on the reduction of the Au precursor at Au(III) absorption maximum.

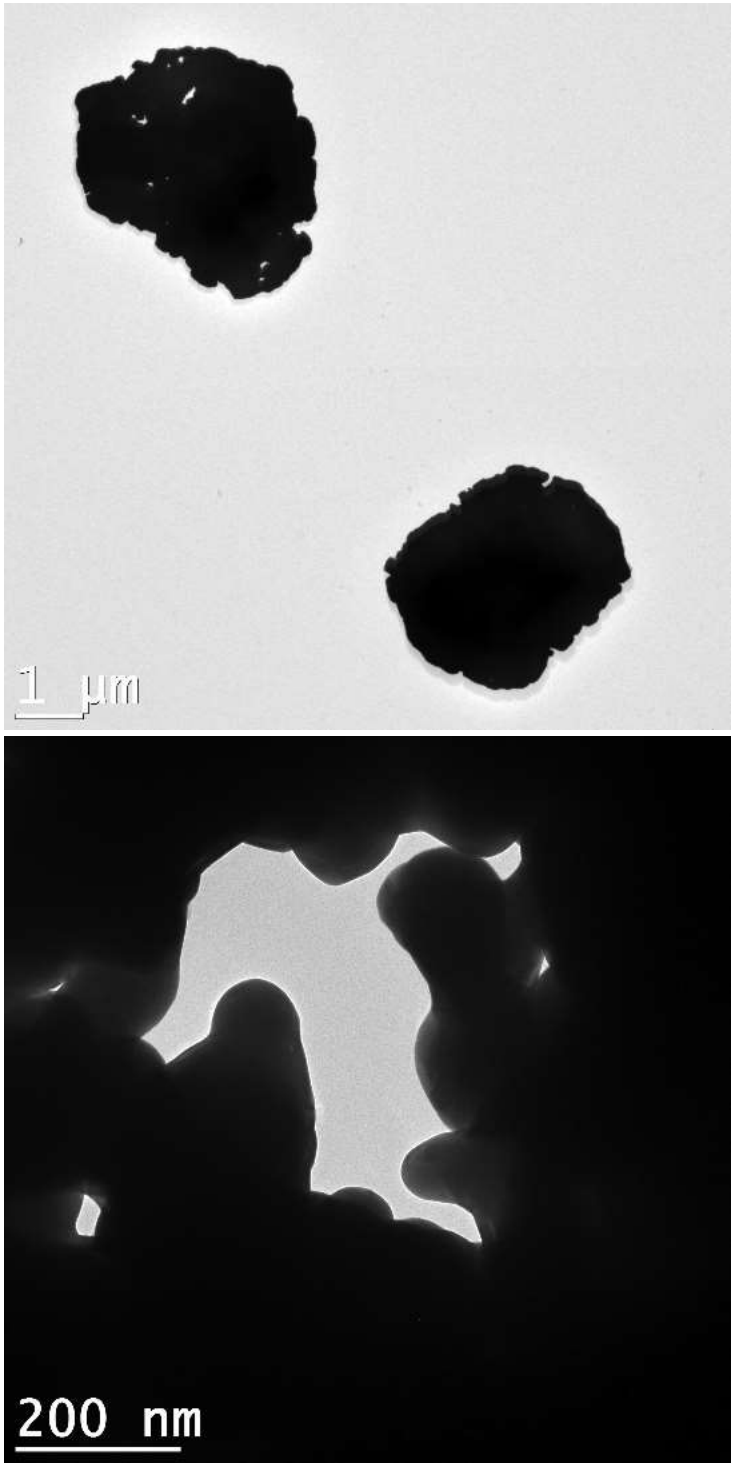

Figure S8. *(A) TEM micrographs of Au MPs obtained from the seed-mediated protocol; GN (Glucose added to NaOH), NG (NaOH added to Glucose); 40 min (sonication time); and I (Intermittent pulse sonication mode). (B) Structural composition of Au MPs.*